Author Manuscript

Author Manuscript

Author Manuscript

Author Manuscript

HHS Public Access

Author manuscript

Nature. Author manuscript; available in PMC 2024 March 08.

Published in final edited form as:

Nature. 2023 March ; 615(7953): 668–677. doi:10.1038/s41586-023-05788-0.

Microglia-mediated T cell Infiltration Drives Neurodegeneration in Tauopathy

Xiaoying Chen[1], **Maria Firulyova**[2], **Melissa Manis**[1], **Jasmin Herz**[3,4], **Igor Smirnov**[3,4], **Ekaterina Aladyeva**[3], **Chanung Wang**[1], **Xin Bao**[1], **Mary Beth Finn**[1], **Hao Hu**[1], **Irina Shchukina**[3], **Min Woo Kim**[3,4], **Carla M. Yuede**[1], **Jonathan Kipnis**[1,3,4], **Maxim N. Artyomov**[3], **Jason D. Ulrich**[1], **David M. Holtzman**[1,4,*]

[1]Department of Neurology, Hope Center for Neurological Disorders, Knight Alzheimer's Disease Research Center, Washington University School of Medicine, St. Louis, MO 63110, USA

[2]Almazov National Medical Research Centre. St Petersburg, Russia

[3]Department of Pathology and Immunology, Washington University School of Medicine, St. Louis, MO 63110, USA

[4]Center for Brain Immunology and Glia (BIG), Washington University School of Medicine, St. Louis, MO 63110, USA

Abstract

Extracellular amyloid-β (Aβ) deposition as neuritic plaques and intracellular accumulation of hyperphosphorylated, aggregated tau as neurofibrillary tangles (NFT) are two of the characteristic hallmarks in Alzheimer's disease (AD)[1,2]. The regional progression of brain atrophy in AD highly correlates with tau accumulation but not amyloid deposition[3–5] and the mechanisms of tau-mediated neurodegeneration remain elusive. Innate immune responses represent a common pathway for the initiation and progression of some neurodegenerative diseases. To date, little is known about the extent or role of the adaptive immune response and their interaction with innate immune response in the presence of Aβ or tau pathology[6]. We systematically compared the immunological milieus in the brain of mice with amyloid deposition or tau aggregation and

*Corresponding author: David M. Holtzman, holtzman@wustl.edu.

Author contribution

XC and DMH conceived the study. XC designed the study, performed the experiments, analyzed the data and wrote the draft of the manuscript. MM, JDU, MBF, JH, JK, XB, MWK, IS and CW were blinded to sample IDs for brain volume, NFL measurement and nesting behavioral assay. MF, EA, XC, MNA and JDU analyzed single cell RNA seq data. HH and XC performed microglia *in vitro* antigen presentation assay. CMY was blinded to sample IDs, performed and analysis the memory behavioral assay. DMH supervised the overall research. XC and DMH wrote the manuscript with comments from all authors.

Data and code availability

Single cell immune sequencing sample information, Alzheimer's Disease patient sample information, immune cell numbers in each cluster in brain are provided in online Supplementary Information. All source data, including sequencing reads and single-cell expression matrices are available from the Gene Expression Omnibus (GEO) under accession code GSE221856.

Code availability

Code for preprocessing of single cell immune sequencing bioinformatic analysis is available from the authors on request.

Conflicts of Interest

D.M.H. is as an inventor on a patent licensed by Washington University to C2N Diagnostics on the therapeutic use of anti-tau antibodies. D.M.H. co-founded and is on the scientific advisory board of C2N Diagnostics. D.M.H. is on the scientific advisory board of Denali and Cajal Neuroscience and consults for Genentech and Alector. J.K. is a member of a scientific advisory group for PureTech. All other authors declare no competing interests.

Author Manuscript Author Manuscript Author Manuscript Author Manuscript

neurodegeneration. We found that mice with tauopathy but not amyloid, developed a unique innate and adaptive immune response and that depletion of microglia or T-cells blocked tau-mediated neurodegeneration. T cells, especially cytotoxic T cells, were markedly increased in areas with tau pathology in mice with tauopathy and in the AD brain. T cell numbers correlated with the extent of neuronal loss, and dynamically transformed their cellular characteristics from activated to exhausted states along with unique TCR clonal expansion. Inhibition of IFN-γ and PD-1signaling both significantly ameliorated brain atrophy. Our results thus reveal a tauopathy and neurodegeneration-related immune hub involving activated microglia and T cell responses, which could serve as therapeutic targets for preventing neurodegeneration in AD and primary tauopathies.

To explore the disease microenvironment in the presence of amyloid (Aβ) or tau deposition, we systematically compared the immunological milieus in the brains of Aβ depositing mice APP/PS1–21(A/PE4) and 5xFAD (5xE4)[7–10], and tauopathy (TE4) mice[11] that express human APOE4 (E4). The pathologies in these models mirror amyloid deposition and tau aggregation with neurodegeneration, respectively[12]. We observed significant brain regional atrophy by 9.5 months but not at 6 months of age in TE4 mice (Fig. 1a). In addition, brain atrophy was not present in A/PE4 nor 5xE4 mice by 9.5 months of age despite massive Aβ deposition in the brain (Fig. 1a and Extended Data Fig. 1a). The atrophy in the TE4 mice at 9.5 months primarily occurred in regions that developed the most tauopathy (i.e. the hippocampus, piriform/entorhinal cortex, and amygdala) and was accompanied by significant lateral ventricular enlargement (Fig. 1a–d and Extended Data Fig. 1b–d). The granule cell layer in the dentate gyrus (DG) as assessed by NeuN staining was noticeably decreased in TE4 mice, and the thickness correlated highly with hippocampal volume (Extended Data Fig. 1e–g). Consistent with the neuronal loss, myelin basic protein (MBP)-positive staining, which is present around intact axons, was altered in TE4 mice at 9.5 months (Extended Data Fig. 1h, 1i). Both TE4 and TE3 (expressing human APOE3) mice developed prominent brain atrophy with somewhat greater atrophy in the TE4 mice (Extended Data Fig. 1j–l). Additionally, male mice tended to have higher levels of brain atrophy than that of females (Extended Data Fig. 1m–o). For further exploration of mechanisms of brain atrophy/neurodegeneration, we focused on male mice for the remainder of the experiments.

Dysregulated innate and adaptive immune responses contribute to some neurodegenerative diseases[13,14]. Neuroinflammation is present in the brain of individuals with AD, and many studies focus on the cellular and molecular changes and the role of microglia, a key component of the innate immune response in the brain during AD development and progression[15]. Microglia are brain resident cells, which may lead to a pro- or anti-inflammatory milieu within the brain together with monocytes, monocyte-derived macrophages and dendritic cells (DCs)[16–18]. T cells and natural killer cells (NKs), if present, are more directly linked with cytotoxicity, and could potentially contribute to neuronal loss in a pro-inflammatory environment[19–22]. Recent studies found an increase of T cells in the cerebrospinal fluid, leptomeninges, and hippocampus in AD[23,24] patients and in mouse models[25,26].

Author Manuscript Author Manuscript Author Manuscript Author Manuscript

Brain and immune cells continuously surveil the environment and make on-demand adjustment to maintain their homeostasis[6,27]. State and functional mapping of these cell types in single cell resolution provide a foundation for understanding brain in health and disease[28]. To map a full picture of the innate and adaptive immune responses in the presence of Aβ or tau pathology, we generated a cellular and molecular atlas of the meningeal and parenchymal immune cell niche via single cell immune sequencing (scRNA-seq) on sorted total CD45-positive cells ($CD45^{Total}$) from meninges and $CD45^{Total}$ and CD45-high cells ($CD45^{high}$) cells from the brain parenchyma in APOE4 knockin mice (E4), A/PE4 and TE4 male mice at 9.5 months with matched genetic background (Fig. 1e, Extended Data Fig. 2a and Extended Data Table 1). Unsupervised clustering identified 12 robust cell types of $CD45^{Total}$ in the parenchyma of E4, A/PE4 and TE4 mice, i.e. microglia, T cells, neutrophils, proliferating cells, B cells, DCs, NK cells, macrophages, $\gamma\delta$ T cells, innate lymphocyte cells (ILCs) and mast cells (Fig. 1f). Surprisingly, the percentage of the T cell population of the total immune cells was strongly increased in the TE4 mice as compared with A/PE4 and E4 mice (Fig. 1g and Extended Data Table 3). In fluorescence activated cell sorting (FACS) analysis, the proportion of $CD45^{high}$ cells, which mainly represents the adaptive immune cell populations and innate immune cells such as DCs and macrophages, were enriched in the brain parenchyma of 9.5 month TE4 mice (Fig. 1e and Extended Data Fig. 2a, 2c and 2d). Consistent with scRNAseq data, we observed a significant increase in CD4 and CD8 T cells in TE4 *vs.* E4 mice, and CD8 cells were the more abundant population (Extended Data Fig. 2b). The meninges are a triple layer structure enveloping the brain and are an immune blood-brain interface[29]. During aging and neurodegenerative diseases, dysfunctional lymphatic vessels lead to impaired drainage, which appears to result in dysregulated immune cell trafficking[30,31]. Distinct cell types were observed in $CD45^{Total}$ populations and the diversity and relative abundance were consistent with previous studies[32] (Fig. 1h, 1i and Extended Data Fig. 2e). In addition, the peripheral T cell composition as assessed in the spleen was not significantly changed in TE4 mice as compared to E4 and A/PE4 mice (Extended Data Fig. 3a–b). Together, these results reveal comprehensive and distinct innate and adaptive immune niches present in the parenchyma and an increased proportion of T cells in the presence of tauopathy and neurodegeneration.

Increased T cells with tau pathology

To further investigate the apparent expansion of T cells observed in our scRNA-seq data, we performed immunohistochemical analyses of the parenchyma from TE4, A/PE4 and 5xE4 mice using antibodies to cluster of differentiation 3 (CD3) and ionized calcium binding adaptor molecule 1 (Iba1), pan markers for T cells and microglia, respectively. We found that T cells were significantly elevated in 9.5 month TE4 mice, but not in 9.5 month E4 controls or in 6-month-old TE4 mice (Fig. 2a, 2b and Extended Data Video. 1). Increased T cells were also found in TE3 mice (Extended Data Fig. 3c) and Tau mice expressing mouse ApoE, suggesting a linkage between T cells and tau-mediated neurodegeneration rather than requiring a specific ApoE isoform. Interestingly, T cells were not obviously increased in amyloid-depositing A/PE4 and 5xE4 mice at 9.5 months of age or even at 19 months of age compared with TE4 mice (Fig. 2a–c). Of note, CD3 staining was primarily present in hippocampus and piriform/entorhinal cortex, which are regions with hyperphosphorylated

Author Manuscript Author Manuscript Author Manuscript Author Manuscript

tau accumulation and neuronal loss, indicating a possible detrimental role for T cells in tau-dependent neurodegeneration (Extended Data Fig. 3d). In accordance with the increase of infiltrated T cells, microglia were also significantly elevated in 9.5 month TE4 mice in regions with brain atrophy (Fig. 2a, 2d). The number of T cells showed a positive correlation with the number of microglia (Fig. 2e) and negatively correlated with the granule cell layer thickness in DG (Fig. 2f). To assess whether the T cells were localized in the brain parenchyma as opposed to within the vasculature, we co-stained brain vessels by retro-orbital Lectin-dye injection and CD3, and noted that $CD3^+$ cells were not present in the lumen of blood vessels (Fig. 2c). Furthermore, transmission electron microscopy (TEM) also revealed that T cells were in the parenchyma adjacent to other cells in the brain (Extended Data Fig. 3e). To determine whether a similar tau pathology-associated increase of T cells is present in the parenchyma in human AD, we performed immunohistochemical analyses in brain samples of AD patients (superior frontal gyrus) with low (I-II) and high (VI) Braak stages (Fig. 2g and Extended Data Table 2). In line with the amount of phosphorylated tau (p-Tau) pathology, $CD3^+$ T cells were strongly elevated in the superior frontal gyrus from Braak stage VI *vs.* the Braak stage I or II cases (Fig. 2g, 2h, 2i). By contrast, in these samples, overall Aβ deposition was similar in brain tissues with both low and high Braak stages (Fig. 2g, 2j). Together, these data demonstrate increased parenchymal T cells are present in brain regions with tauopathy but not in the presence of only amyloid deposition in both humans and mice.

T cells shift states with tau pathology

To depict the cellular and molecular signatures of the T cells in the presence of Aβ or tau pathology, we assessed T cell populations from single cell immune RNA-seq data from $CD45^{high}$ cells in the parenchyma and $CD45^{Total}$ cells in the meninges in E4, A/PE4 and TE4 mice. T cells were categorized into 15 subgroups across all samples based on expression of featured genes (Fig. 3a, Extended Data Fig. 4a and Extended Data Table 3). Cell population analysis revealed population differences between parenchyma and meninges. Naïve $CD8^+$ T cells (subgroup 11), $Folr4^+CD4^+$ T cells (subgroup 4) and Regulatory T cells (subgroup 13) were highly enriched in meninges, but effector $CD8^+$ T cells (subgroups 3, 8, 10) were preferentially enriched in brain parenchyma (Fig. 3b). These results suggest that brain-border and brain-resident T cells are functionally different in accordance with their immune niche. Interaction between the T cell receptor (TCR) and antigens presented by the major histocompatibility complex (MHC) is critical to adaptive immunity[33]. T cells clonally expand, when they recognize cognate antigen[34]. We next performed single cell TCR sequencing (scTCR-seq) on T cells, which showed unique T cell clonal enrichment in the parenchyma with tauopathy and neurodegeneration (Extended Data Fig. 4b–d). We evaluated TCR repertoires among $CD4^+$ T cell subsets and observed an increased clonality in $CD4^+$ T cells in TE4 mice that was concentrated within the activated $CD4^+$ T cells ($Nkg7^+Ccl5^+$ and $Cxcr6^+Ccr8^+CD4^+$ T cells) (Fig. 3c–e). Similar to what we found in $CD4^+$ T cells, paired TCRα/TCRβ repertoire analysis revealed TCR clonal expansion in $CD8^+$ T cells in TE4 mice (Fig. 3f). Unsupervised clustering identified 10 robust cell types in $CD8^+$ T cells (Fig. 3g, Extended Data Fig. 4a and Extended Data Table 3). Activated $CD8^+$ T cells ($CD11c^+$ $Klre1^+$ and $Isg15^+$ $CD8^+$ T cells) were more abundant in TE4 mice, while

Author Manuscript Author Manuscript Author Manuscript Author Manuscript

the fraction of Tox^+ $Pdcd1^+$ $CD8^+$ exhausted T cells were slightly decreased, suggesting a potential role of activated $CD8^+$ T cells in mediating neuronal loss in tauopathy (Fig. 3h). Pseudotime analysis of $CD8^+$ T cells found a range of T cell states indicative of a dynamic shift from activated to exhausted states (Fig. 3i). We also observed an increased clonality in activated and exhausted $CD8^+$ T cells in TE4 mice (Fig. 3j). Together, these data illustrate T cells in the brain parenchyma dynamically shift from activated to exhausted states with unique TCR clonal expansion in both $CD4^+$ and $CD8^+$ populations in the brain in a mouse model of tauopathy.

Interaction of microglia and T cells

We next explored the unique but complex immune hubs in the parenchyma of tauopathy brains, which lead to T cell homing and activation. Notably, CCL3, CCL4 and CXCL10, chemokines previously reported to be associated with T cell chemotaxis and brain infiltration were increased in the brain lysates of TE4 mice compared to E4 and TEKO (P301S Tau:ApoE KO) mice[25,35] (Extended Data Fig. 5). Microglia are the first responders to neuroinflammation or damage and they rapidly adapt their phenotypes and functions in response to the dynamic brain milieu[36]. Typical functions of microglia such as phagocytosis and cytokine production have been well characterized in models of neurodegeneration including AD[37,38]; however, whether they exert their effects via their interactions with T cells is largely unknown. We sub-grouped microglia (cell type 0, Fig. 1f) from the $CD45^{Total}$ population of E4, A/PE4 and TE4 mice and obtained 3 subgroups with distinguishing markers associated with homeostatic microglia (HOM), disease associated microglia (DAM) and interferon-activated microglia (IFN) (Fig. 4a, 4b). Notably, DAM and IFN subgroups were strongly elevated in TE4 mice, while the HOM subgroup decreased (Fig. 4c and Extended Data Table 3). We found genes related to antigen presentation, complement response and cytokines, metabolism and oxidative stress, together with lysosomal enzymes were upregulated in TE4 mice to a greater extent compared to A/PE4 mice, which were greater than the control mice (Fig. 4d). Classically, MHCI and MHCII enable antigen presentation to $CD8^+$ T cells and $CD4^+$ T cells, respectively. MHCI is expressed by all nucleated cells, while MHCII is only expressed by antigen presenting cells (APCs), such as DCs, macrophages, B cells and microglia[39]. By co-staining with the perivascular macrophage marker, MRC1 mannose receptor C (CD206), in addition to MHCII, Iba1 and GFAP, we found MHCII was primarily present in $Iba1^+$ microglia in the brain parenchyma in neurodegeneration regions (Extended Data Fig. 6a). Indeed, in line with the increase in parenchymal T cells, we found that $MHCII^+$ microglia were significantly elevated in brain regions with tau pathology in TE4 mice (Extended Data Fig. 6b, 6c). DAM and its sub-types have been well characterized in amyloid models[40]. Here, in TE4 mice, we found Integrin, α_X (CD11c) positive microglia, a representative marker for myeloid cell 2 (Trem2)-dependent type 2 DAM, physically co-localized with $CD8^+$ T cells (Extended data video. 2). Interestingly, CD11c was also strongly increased in TE4 hippocampus as compared to the A/PE4 and E4 control mice (Extended Data Fig. 6d, 6e). These results highlight a tight correlation with $MHCII^+$ microglia, $CD11c^+$ microglia, T cells and neurodegeneration. Sparse $MHCII^+$ microglia and $CD11c^+$ microglia were also found co-localized with parenchymal plaques in A/PE4 mice (Extended Data Fig. 6b, 6d). ApoE

Author Manuscript Author Manuscript Author Manuscript Author Manuscript

deletion rescued brain atrophy in TEKO mice and MHCII$^+$ and CD11c$^+$ microglia as well as T cells were significantly decreased (Extended Data Fig. 6 b–g). The higher inflammatory reactivity associated with Tau-mediated neurodegeneration and ApoE were also confirmed by assessment of inflammatory cytokines in brain tissue from TE4 and TEKO mice (Extended Data Fig. 5). Together, these data demonstrate that parenchymal microglia, in the presence of tauopathy, shift their transcriptomic and phenotypical states from homeostatic to disease-associated, CD11c$^+$, MHCII$^+$ and IFN-activated states, with accompanying increase in inflammatory chemokines and cytokines.

IFN-γ, a cytokine upregulated in TE4 mice, is a proinflammatory cytokine produced by NK, NKT, and T cells that can prime microglia for inflammatory responses to injury as well as promote cytotoxic CD8$^+$ T cell function[6]. Previous studies identified IFN-γ related transcriptomic signatures in tauopathy and neurodegenerative disease models, although the cell-type expression and functional result of IFN-γ on pathology was not described[41]. Ligand-receptor analysis revealed active interactions within T cells and microglia (Extended Data Fig. 7a). IFN-γ receptor was already known to be expressed in both neurons and microglia in the brain[42]. Importantly, we found that in the brain of TE4 mice, IFN-γ transcripts were enriched in T cells, especially CD8$^+$ T cells (Extended Data Fig. 7b). Given that IFN-γ can augment antigen presenting and inflammatory functions of myeloid cells, we further investigated the role of IFN-γ in the immune response in tauopathy. To determine whether microglia can present antigen to T cells *in vitro*, we co-cultured microglia acutely isolated from adult mouse brain with OT-1 T cells, with soluble ovalbumin (OVA) as antigen, and found that microglia were capable of weakly stimulating OT-1 T cell proliferation compared to DCs (Extended Data Fig. 8c–f). However, upon IFN-γ stimulation, OT-1 T cell proliferation was strongly enhanced in the presence of microglia with OVA (Extended Data Fig. 8e, 8f), nearly to the level observed with DCs, suggesting that microglia *in vitro* can serve as antigen presenting cells and that IFN-γ can augment this response. Together, these data suggest the possibility that there are active interactions between microglia and infiltrated T cells.

To determine the role of endogenous IFN-γ in the P301S mice *in vivo* and to study the interplay between activated microglia and T cells, we blocked IFN-γ signaling by peripheral administration i.p. every five days with a neutralizing antibody in TE3 mice from 7.5 to 9.5 months of age, right before T cell infiltration into the brain parenchyma. Anti-IFN-γ (αIFN-γ) treatment resulted in attenuated brain atrophy as compared to the IgG treatment control (Extended Data Fig. 8a–d). CD11c$^+$ microglia were also significantly reduced in αIFN-γ treated mice (Extended Data Fig. 8e, 8f) and there was a significant reduction in p-Tau staining in αIFN-γ treated mice (Extended Data Fig. 8g, 8h). Taken together, these results suggest that IFN-γ secreted by CD8$^+$ T cells in the brain can augment tau pathology and neurodegeneration, at least in part through promoting inflammatory microglial signaling and antigen presentation functions.

To further delineate the interrelationship between the activated microglia and infiltrated T cells, we administered PLX3397, a selective CSF1R/c-kit/FLT3 inhibitor, in TE4 and E4 control mice from 8.5 months to 9.5 months of age (Extended Data Fig. 9i). PLX3397 treatment resulted in strong microglial depletion (Fig. 4e–k). PLX3397 treatment also

Author Manuscript Author Manuscript Author Manuscript Author Manuscript

decreased hippocampal atrophy and ameliorated the increased of ventricular volume in TE4 mice (Fig. 4l–o). Notably, $CD3^+$ and $CD8^+$ T cells as well as tau pathology were reduced upon microglia depletion (Fig. 4p–r), suggesting a pivotal role of microglia, especially activated microglia, in setting of the tauopathy-specific immune hubs by recruiting and activation T cells into the brain parenchyma and a detrimental role of this re-structured immune hub in facilitating disease progression.

T cell depletion prevent degeneration

To directly investigate whether infiltration of T cells leads to neurodegeneration, we depleted T cells by peripheral administration of neutralizing antibodies in TE4 mice as well as their age-matched non-tau transgenic littermates from 6 months to 9.5 months of age, a critical time window when neurodegeneration develops (Extended Data Fig. 8j). A single dose acute i.p. treatment with anti-CD4 (αCD4) and anti-CD8 (αCD8) antibodies (αT) led to strong CD4 and CD8 T cells depletion in brain parenchyma, meninges and peripheral blood, confirming the antibody depletion efficiency (Extended data Fig. 9a, 9b). Strikingly, in TE4 mice with αT treatment (i.p. every 5 days) from 6 months to 9.5 months, brain atrophy was strongly ameliorated compared to IgG treated control (Fig. 5a–d). T cells were almost completely eliminated in the brain parenchyma in TE4 mice after 3.5 months of αT antibody treatment (Fig. 5e, 5g, 5h, 5i). Interestingly, T cell depletion also reduced overall microglial staining (Fig. 5e, 5f, 5g, 5j), suggesting that T cells in the brain of TE4 mice can augment microgliosis. To assess the activation status of microglia with and without T cells depletion, we performed immunohistochemical analyses of the parenchyma from TE4-IgG and TE4-αT treated mice using antibodies to P2ry12, MHCII and CD11c (Fig. 5f, 5g). We found significant elevation of $P2ry12^+$ microglia and reduced $MHCII^+$ and $CD11c^+$ microglia (Fig. 5k–m) in the αT antibody treated mice, suggesting microglia shift from activated towards a more homeostatic state after T cell depletion. Single cell RNA seq analysis of microglia from αT antibody *vs.* the IgG control treated mice also revealed strong suppression of different aspects of the disease related microglia signature and an increase in the homeostatic signature (Extended Data Fig. 9c–e). To assess tau pathology following T cell depletion, we analyzed p-Tau immunoreactivity in hippocampus and found a significant reduction in p-Tau in αT treated mice (Fig. 5n). Four major p-Tau staining patterns, designated as type1–4, strongly correlated with the level of brain atrophy, with type 1 associated with most preserved brain tissue and type 4 associated with the greatest atrophy. Depletion of T cells resulted in a significant shift of p-Tau staining pattern toward the earliest disease stage (Fig. 5o, 5p). We also assessed plasma protein levels of neurofilament light chain (NfL), a marker of neuroaxonal damage and neurodegeneration[43]. NfL concentration in T cell depleted mice was significantly reduced (Fig. 5q). Behavioral performance assessment revealed that after depletion of T cells, nest-building behavior in 9.5 month TE4 mice was significantly improved (Extended Data Fig. 10f). We also assessed an additional cohort of TE4 mice that we treated with αT antibody *vs.* the IgG control from 6 months to 8.5 months of age. Assessment of behavioral performance revealed that depletion of T cells resulted in significant improvement in 2 additional behaviors. Y maze alternation, assessing short-term memory and exploratory behavior, as well as freezing in response to auditory cue, assessing amygdala-dependent memory, were significantly improved (Fig. 5r–

Author Manuscript Author Manuscript Author Manuscript Author Manuscript

u and Extended Data Fig. 9g–i). Freezing behavior in response to a contextual cue showed a trend toward increased hippocampal dependent memory after depletion of T cells (Fig. 5t). Both groups showed similar baseline levels of general exploratory behavior, and locomotor activity levels (Extended Data Fig. 9g–h) and response to tone/shock pairing in the fear conditioning test (Fig. 5s). Together, these data demonstrate that T cell depletion decreases functional decline.

Immune checkpoints are regulatory pathways for maintaining systemic immune homeostasis and tolerance[44]. Programmed death (PD)-1 is a checkpoint protein expressed on T cells, which processes inhibitory signals to control the magnitude of adaptive immune responses and tolerance[45]. Previous reports indicate that PD-1 immune checkpoint blockade decreases cognitive impairment in mouse models with AD pathology[46,47]. PD1 blockade can lead to increased activation of exhausted CD8 T cells or enhanced immunosuppression through increased activation of $PD1^{+}CD4^{+}$ Tregs[48]. To investigate whether a treatment that targets PD-1/PD-L1 blockade could be effective in tauopathy, we administered anti-PD-1 (αPD-1) treatment in TE4 mice from 8 months to 9.5 months of age, a time window that brain atrophy dramatically develops. We found that with one-week acute αPD-1 treatment increased percentage of $Foxp3^{+}CD4^{+}$ Tregs and $Pd1^{+}Foxp3^{+}CD4^{+}$ Tregs, with no obvious changes on $Klrg1^{+}$ effector $CD8^{+}$ T cells and total $Pd1^{+}Tox^{+}$ $CD8^{+}$ T cells in the brain (Extended Data Fig. 10 a–e). These results suggest that PD1-antibody treatment at this age would increase immunosuppressive CD4 Tregs. Consistent with this hypothesis, chronic treatment beginning at 8 months significantly decreased tau-mediated neurodegeneration and p-Tau staining (Extended data Fig. 10f–i), further supporting a role for T cells in tau-mediated neurodegeneration.

In this study, we present a comprehensive cellular and molecular immune response map in the brain and meninges during the development of amyloid or tau pathology and neurodegeneration via scRNA-seq and scTCR-seq. We find that an immunological hub involving activated microglia and T cells are overrepresented in brain regions with tauopathy and neuronal loss. Though evidence regarding the pathological changes and the role of microglia in AD are emerging, here, we expand on the immune microenvironment in tauopathy by assessing a previously less examined adaptive immunological response and their interaction with cells in the brain. T cells dynamically shift from activated to exhausted states with unique TCR clonal expansion. More importantly, we present direct evidence that breaking the neurodegeneration-featured immune hub between activated microglia and infiltrated T cells effectively prevents neurodegeneration and improve cognitive decline in AD and primary tauopathies.

As an innate primary response, microglia appear to play an anti- (restrict plaque and inflammation expansion) or pro-inflammatory (response to neuronal damage and aggregated tau and lead to severe neurodegeneration) role in AD[12]. Here, we found CD11c and MHCII expression strongly increased in microglia specifically in brain atrophy regions. MHCI and MHCII complex genes were highly upregulated in activated microglia in tauopathy. More importantly, as adaptive responses, we discovered that within both a mouse model of tauopathy and AD patient brain samples, T cells are not only present in the brain parenchyma but their enrichment also highly correlates with the severity of brain atrophy.

Author Manuscript Author Manuscript Author Manuscript Author Manuscript

Removal and modulation of T cells rescued the brain atrophy and highlighted that T cells play an important role in neurodegeneration.

The complex nature of the central nervous system (CNS) necessitates its own specialized immunological adaptations to detect and respond to environmental changes. Here we found significantly different proportions of T cells in the meninges and brain parenchyma. These results highlight that CNS-border and CNS-resident T cells are functionally different in accordance with their immune niche. The local tauopathy-related microenvironment in the brain parenchyma is likely to be instructive for recruiting and guiding the transformation of T cells. The interaction of T cells with APCs has been well established in peripheral systems[49] and CNS-borders[32]. Here, our findings raise a fundamental question regarding the interaction of T cells with APCs in the brain parenchyma. We find that T cells actively interact with the disease related microglia subgroups. Depletion of microglia largely abolishes T cell infiltration and depletion of T cells also remarkably hinders microglia activation, strengthening immunological communication between the innate and adaptive family of immune cells. In combined scRNA-seq and scTCR-seq analyses, we uncover unique T cells clonal expansion enriched in the parenchyma with tauopathy and neurodegeneration. To understand which specific antigens are resulting in T-cell infiltration, such as variously modified forms of tau, other proteins or myelin debris released by damaged neurons are presented to adaptive immune cells within tauopathy and AD remains an intriguing question. Sequencing TCRs at the single cell level combined with high-throughput peptide screening would enable elucidation of the specific antigens, which might in turn yield pathological stage-specific therapeutic strategies. Microglia express many pattern recognition receptors (PRRs) that bind and internalize foreign misfolded proteins[50]. We found T cell infiltration did not increase in the Tau mice lacking ApoE. Therefore, a previously overlooked immunomodulatory function of ApoE may serve as an important mechanism linking both innate and adaptive immunity. Mapping the disease state-specific interlink between microglia and T cells, including their signaling communications, presented antigens, and pathophysiological responses will be a key nexus to set up unique therapeutic interventions to prevent or reverse brain atrophy in tauopathies.

Online-only Methods

Animals

Human ApoE knock-in mice, ApoE3 and ApoE4 (E3 and E4, respectively), were generated by replacing the mouse genomic sequence from the translation initiation codon in exon2 to the termination codon in exon4 with its human counterparts flanked by loxP sites[51]. P301S tau transgenic mice (Jax, #008169) on C57BL/6 background were crossed to human ApoE KI or ApoE KO mice (Jax, #002052) to generate P301S/E3 (TE3), P301S/E4 (TE4), and P301S/EKO (TEKO) mice respectively. All tau transgenic mice involved in the final analysis were obtained from the same generation. A/PE4 and 5XFADE4 mice have been described[8,51]. Littermates of the same sex were randomly assigned to experimental groups. All animal procedures and experiments were performed under guidelines approved by the Institutional Animal Care and Use committee (IACUC) at Washington University School of Medicine.

Author Manuscript Author Manuscript Author Manuscript Author Manuscript

Human AD tissues

All participants gave prospective pre-mortem written consent for their brain to be banked and used for research with information to potentially be published under procedures approved by the human institutional review board at Banner Sun Health Research Institute. Patient demographics can be found in Extended Data Table 2.

Volumetric analysis

The left hemi-brain of each mouse was fixed by 4% paraformaldehyde for 24 h at 4 °C and then placed in 30% sucrose at 4 °C overnight. Serial free-floating coronal sections were cut from the rostral crossing of the corpus callosum to the caudal end of the hippocampus at 50 μm on a Leica SM2010 microtome. Brain sections (spaced 300 μm apart) from bregma −1.3 mm to −3.1 mm were mounted for volumetric analysis. All mounted sections were stained with 0.1% Sudan black (Sigma, 199664–25G) in 70% ethanol at RT for 20 min, washed in 70% ethanol for 50s, 3 times. The sections were washed in Milli-Q water 3 times and covered with Floromount-G (Southern Biotech, 0100–01). Slides were scanned using Hamamatsu's NanoZoomer microscope at 20x magnification. Hippocampus, Ent/Piri cortex and ventricles were traced using NDP viewer. The volume was calculated using formula: volume= (sum of area) x 0.3 mm.

Immunohistochemistry

Two sections from each mouse (300 μm apart), corresponding approximately to bregma coordinates −1.4 mm, −1.7 mm were used for p-tau staining. Brain sections were washed in Tris-buffered saline (TBS) buffer for 3 min followed by incubation in 0.3% hydrogen peroxide in TBS for 10 min at RT. After 3 times washing in TBS, sections were blocked by 3% milk in TBS with 0.25% Triton X-100 (TBSX) for 1h at RT followed by incubation with AT8-biotinylated antibody (Thermo Scientific, MN1020B) overnight at 4 °C. The next day, after 3 times washing in TBS, the slices were developed by VECTASTAIN Elite ABC-HRP kit (Vector laboratories, PK-6100) following the manufacturer's instructions. Slides were covered by cytoseal60 (Thermo Scientific, 8310–4) and scanned using a Hamamatsu NanoZoomer microscope at 20x magnification. Images were analyzed by ImageJ.

For immunofluorescent staining, two sections (bregma −2.0 mm and −2.3 mm) from each mouse were used. The sections were washed in TBS 3 times, permeabilized with 0.25% TBSX for 10 min, followed by blocking with 3% BSA in 0.25% TBSX for 1h at RT. Sections were incubated in primary antibodies overnight at 4 °C. The next day, sections were washed in TBS and incubated with corresponding fluorescence-labeled secondary antibodies for 1.5 h at RT. The slices were washed and mounted in prolong gold antifade mounting media (Invitrogen, P36930). Primary antibodies were as follows: CD3 (Novus, NB600–1441, 1:200), CD8 (Invitrogen, MA1–145, 1:100), Iba1(Wako, 019–19741, 1:2000; Abcam, ab5076, 1:500), AT8 (Invitrogen, MN1020B, 1:500), Aβ (Homemade, HJ3.4B, 1:1000), P2ry12 (Gift from Butovsky lab, 1:2000), NeuN (Abcam, ab177487, 1:1000), MBP (Abcam, ab7349, 1:500), MHCII (Biolgend, 107650, 1:200), X34 (Sigma, 1954–25MG, 10mM in DMSO stock, 1:5000), CD206 (Bio-Rad, MCA2235, 1:300), Hoechst (sigma, 94403, 1:5000). Secondary antibodies were as follows: Donkey anti-Rat 488 (Invitrogen, A21208, 1:500), Donkey anti-Rabbit 405 (Invitrogen, A48258, 1:500), Donkey anti-Rabbit

Author Manuscript Author Manuscript Author Manuscript Author Manuscript

568 (Invitrogen, A10042, 1:500), Streptavidin 568 (Invitrogen, S11226, 1:500), Donkey anti-Goat 647 (Invitrogen, A21447, 1:500). Images were acquired on a Zeiss LSM800 microscope. Antibody-fluorophores covered area and numbers were analyzed by ImageJ. 3D construction was performed using Imaris 9.7.0 software. CD3, IBA1, CD8 and CD11c were labeled and detected with fluorophores using surface area function.

PLX3397 formulation and supplement

PLX3397 was purchased from SelleckChem. PLX3397 was formulated in the AIN-76A (Research Diet) at a concentration of 400mg/kg chow. E4 and TE4 mice were treated with PLX for 4 weeks for microglial acute depletion from 8.5 to 9.5 months of age.

IFN-γ treatment

For blocking IFN-γ signaling, mice were i.p. injected with 100mg/kg body weight with either control IgG (Leinco, P376) or anti-mouse IFN-γ (Leinco, clone H22, I-1190) antibodies[52] every 5 days from 7.5 to 9.5months of age.

Anti-PD-1 treatment

For blocking PD-1/PD-L1 signaling chronically, mice were i.p. injected with 500μg anti-PD-1 antibody (BioXCell, BP0146) every 5 days from 8 to 9.5 months of age. IgG (BioXCell, BP0089) isotype control was administered at the same frequency and dosage. Brains were collected for flow cytometry assessment of T cell populations. To characterize the T cell populations with anti-PD1 treatment, mice were acutely treated with 500 μg anti-PD1 or IgG every 2 days. At day7, after perfusion, brain were isolated for single cell for flow cytometry. Intracellular staining for transcription factors was performed using eBioscience FOXP3/Transcription Factor Kit (Ref. 00–5523-00) per manufacturer's instructions. In brief, cells were stained with LIVE/DEAD Fixable Aqua Dead Cell Stain Kit (Invitrogen, Ref. L34966A) for 5 min and then incubated with surface antibody mix and TruStain FcX PLUS (anti-mouse CD16/CD32, Clone S17011E, Biolegend, Ref. 156604, 1:200) for 1 h at room temperature. After cell-surface staining, cells were fixed, permeabilized, and incubated with intracellular antibody mix overnight at 4°C. Flow cytometry was performed on a BD Symphony A3. The following antibodies were used. Biolegend: CD45.2 (104), CD4 (GK1.5), Pd1 (29F.1A12), Klrg1 (2F1/KLRG1). BD: CD3e (145–2C11), CD8a (53–6.7). Invitrogen: Foxp3 (FJK-16s), Tox (TXRX10).

T cell depletion

For the depletion of $CD4^+$ and $CD8^+$ T cells, mice were i.p. injected with 500μg anti-CD4 (BioXCell, BP0003–1) and anti-CD8 antibody (BioXCell, BP0061) every 5 days from 6 to 9.5 months of age or for memory related behavioral experiments from 6 to 8.5 months of age. IgG (BioXCell, BP0090) isotype control was administered at the same frequency and dosage. To characterize the depletion efficiency, mice were acutely treated with 500 μg anti-CD4, or anti-CD8 or IgG. Brain, meninges and blood were extracted for single cell analysis followed by flow cytometry assessment of $CD4^+$ and $CD8^+$ T cell populations.

Author Manuscript Author Manuscript Author Manuscript Author Manuscript

Brain extraction

Mouse cortex tissue was weighed and homogenized using a pestle with 10μl buffer/1mg tissue in chilled lysis buffer (Thermo Scientific, 78503). After centrifugation at 20,000 g for 10 min at 4 °C, the supernatant was saved and protein concentration was measured by micro BCA protein assay kit (Thermo Scientific, 23235) before multiplex immunoassay (Thermo Scientific).

Nest-building behavior

Group-housed mice were switched to individual housing in the week of assessment at 9.5 months. Pre-weighted nestlet was provided in each cage. After an overnight housing, the remaining nestlet was weighted. The 5-point scale system was included and given based on percentage of remaining nesting material and shredded conditions. Score 1: nestlet >90% untorn; score 2: 50–90% of nestlet is untorn; score 3: 10%−50% of nestlet is untorn; score 4: nestlet <10% untorn, but nest is flat and uncompact; score 5: nest is compact and nest wall is higher than the mouse for >50% of its circumference.

General Design of Behavioral Tests

TE4 male mice were treated with IgG or with anti-CD4 and anti-CD8 antibodies for T cell depletion from 6 to 8.5 months of age. They were then tested for behavioral differences. Following 1 week habituation and handling in the Washington University Animal Behavior Core, mice were evaluated on 1 hour locomotor activity, spontaneous alternation in a Y maze, and fear conditioning. All tests were conducted during the light phase of the light/dark cycle. Behavioral testers were blind to the treatment group.

One-hour locomotor activity and open-field behavior test

To evaluate general activity levels and possible alterations in emotionality, mice were evaluated over a 1-h period in transparent (47.6 × 25.4 × 20.6 cm high) polystyrene enclosures. Each cage was surrounded by a frame containing a 4 × 8 matrix of photocell pairs, the output of which was fed to an on-line computer (Hamilton-Kinder, LLC, Poway, CA). The system software (Hamilton-Kinder, LLC) was used to define a 33 × 11 cm central zone and a peripheral or surrounding zone that was 5.5 cm wide with the sides of the cage being the outermost boundary. This peripheral area extended along the entire perimeter of the cage. Variables that were analyzed included the total number of ambulations and rearing on hindlimbs, as well as the number of entries, the time spent, and the distance traveled in the center area as well as the distance traveled in the periphery surrounding the center.

Spontaneous alternation Y-maze

Testing was conducted according to our previously published procedures[53]. Briefly, this involved placing a mouse in the center of a Y-maze that contained three arms that were 10.5 cm wide, 40 cm long and 20.5 cm deep where an arm was oriented at 120° with respect to each successive other arm. Mice were allowed to explore the maze for 10 min and entry into an arm was scored only when the hindlimbs had completely entered the arm. An alternation was defined as any three consecutive choices of three different arms without re-exploration of a previously visited arm. Dependent variables included the number of alternations and

Author Manuscript Author Manuscript Author Manuscript Author Manuscript

arm entries along with the percentage of alternations, which was determined by dividing the total number of alternations by the total number of entries minus 2, then multiplying by 100.

Conditioned Fear

A previously described protocol[54] was used to train and test mice using two clear-plastic conditioning chambers (26×18×18 cm high) (Med-Associates, St. Albans, VT) which were easily distinguished by different olfactory, visual, and tactile cues present in each chamber. On day 1, each mouse was placed into the conditioning chamber for 5 min and freezing behavior was quantified during a 2 min baseline period. Freezing (no movement except that associated with respiration) was quantified using FreezeFrame image analysis software (Actimetrics, Evanston, IL) which allows for simultaneous visualization of behavior while adjusting for a "freezing threshold" during 0.75 s intervals. After baseline measurements, a conditioned stimulus (CS) consisting of an 80 dB tone (white noise) was presented for 20 sec followed by an unconditioned stimulus (US) consisting of a 1 s, 1.0 mA continuous foot shock. This tone-shock (T/S) pairing was repeated each minute over the next 2 min, and freezing was quantified after each of the three tone-shock pairings. Twenty-four hours after training, each mouse was placed back into the original conditioning chamber to test for fear conditioning to the contextual cues in the chamber. This involved quantifying freezing over an 8 min period without the tone or shock being present. Twenty-four hours later, the mice were evaluated on the auditory cue component of the conditioned fear procedure, which included placing each mouse into the other chamber containing distinctly different cues. Freezing was quantified during a 2 min "altered context" baseline period as well as over a subsequent 8 min period during which the auditory cue (CS) was presented. Shock sensitivity was evaluated following completion of the conditioned fear test as previously described[55].

NfL concentration

Plasma NfL concentration was measured with NF-Light Simoa Assay Advantage kit, Quanterix.

Single cell isolation

Mechanical dissociation was performed as previously described[56]. Briefly, mice were perfused with pre-chilled PBS to fully remove blood contamination. Hippocampus and cortex were dissected followed by Dounce homogenization. Cell suspensions were then passed through Percoll density centrifugation to remove myelin and debris. The cell pellets were washed with 0.5% BSA for analysis or collection. For meninges, meninges were peeled intact from the skullcap using fine forceps and prepared for single cell analysis as previously described[32]. Briefly, meninges were mashed through a cell strainer, using a sterile syringe plunger and washed in 0.5%BSA.

Flow cytometry for single cell

All steps were performed on ice or using pre-chilled centrifuge set to 4°C. Single cell suspensions were incubated with anti-CD16/32 (Fc block; Bio legend) for 5 min then fluorescently conjugated antibodies were added for 20 min. After washing, samples were

Author Manuscript Author Manuscript Author Manuscript Author Manuscript

collected by 300g followed by a 5min spin down and suspended in 5% BSA with PI for live/Dead selection before sorting. Cells were sorted using FACsAria II (BD Bioscience).

Single cell immune sequencing

After counting and analyzing single cell integrity, 8,000–16,000 individual single cells per sample were loaded onto a 10X Genomics Chromium platform for Gel Beads-in-emulsion (GEM) and cDNA generation carrying cell- and transcript-specific barcodes and sequencing libraries constructed using the Chromium Single Cell 5'library & Gel Bead Kit V2. Libraries were sequenced on the Illumina NovaSeq6000.

Single cell data processing and TCR analysis

Alignment, barcode assignment, and UMI counting with Cell Ranger (v6.1.1) were used for preparation of count matrices for gene expression library. For alignment, a custom mouse genome (GRCm38) containing human sequences for *APOE*, *PSEN1*, *APP*, *MAPT* genes was used as a reference.

Barcodes in all samples that were considered to represent noise and low-quality cells were filtered out using knee-inflection strategy available in default Cell Ranger (v6.1.1) from 10x genomics.

For downstream, Seurat package (v4.0.4) was used, genes which express in less than three cells additionally filtered from expression matrices. The mitochondrial genes fraction was calculated for every cell, and cells with a mitochondrial fraction more than highest confidence interval for scaled mitochondrial percentage were filtered out which results in removal of the cells with mitochondrial percentage more than 20%. Additionally, cut off with log10 (number of unique expressed genes) as 2.5 was used for removing the cells from both $CD45^{High}$ and $CD45^{Total}$ parenchyma cells, and 2 was used as a threshold for the cells from meninges.

Doublets have been excluded based on the co-expression of the canonical cell-type specific genes.

Each sample was normalized using SCTransform function with mitochondrial content as a variable to regress out in a second non-regularized linear regression. For integration aims, variable genes across the samples were identified by SelectIntegrationFeatures function with the number of features equal to 2000. Then the object was prepared for integration (PrepSCTIntegration function), the anchors were found (FindIntegrationAnchors function) and the samples were integrated into the whole object (IntegrateData function).

The principal component analysis was used for dimensionality reduction, and the first 20 principal components (PCs) were used further to generate uniform manifold approximation and projection (UMAP) dimensionality reduction by RunUMAP function. Clustering procedure was performed by FindNeighbors and FindClusters with a range of resolutions (from 0.2 to 1.0 with 0.2 as a step) and the first 20 PCs as input.

Author Manuscript Author Manuscript Author Manuscript Author Manuscript

The object covering all cells has been subsetted into T-cell, microglia and myeloid specific sub-objects based on expression of canonical gene markers. Additionally, the T-cells object was split into $CD4^+$ and $CD8^+$ cells. Then, all objects passed through the iterative process of quality control with doublets removal and exclusion of the cell typess which have no relevant markers and contained high mitochondrial content as well as poor coverage (all filters are object-specific).

Cell Ranger's vdj workflow (v6.1.1) was used for TCR data analysis. Non-canonical T cells (such as gamma-delta T cells and natural killer T cells) as well as T cells with inappropriate combinations of alpha/beta chains were removed. Then, all barcodes were assigned to two populations based on CD4 and CD8 gene expression. The Gini coefficient was calculated using the immunarch package (v0.6.6) in order to estimate the clonal diversity among samples.

Trajectory analysis was done using a slingshot container available at dynverse package with normalized count matrices with barcodes assigned to microglia as input data as well as cells assigned to $CD8^+$ T cells.

Interaction analysis was implemented using the CellChat package (v. 1.1.3) with the "Cell-Cell Contact" database. As input data, microglia, CD4 and CD8 T cells from E4 genotype and microglia, $CD4^+$ and $CD8^+$ T cells from TE4 genotype were used. Following the CellChat vignette, CellChat objects were prepared (createCellChat), overexpressed genes and interactions were identified (identifyOverExpressedGenes, identifyOverExpressedInteractions functions), communication probabilities were estimated (computeCommunProb, filterCommunication, computeCommunProbPathway functions), and network analysis (aggregateNet, netAnalysis_computeCentrality functions) was performed. The genotype-specific as well as genotype-common ligand-receptor pairs were identified (netVisual_bubble function). The number of interactions were evaluated using netVisual_circle function.

Peripheral immune cell composition assay

Spleens from E4, A/PE4 and TE4 mice were collected and smashed through a 70micron strainer to prepare single cell suspensions. After single cell suspensions were made, the cells were pelleted down and resuspended in 5ml red blood cell lysis buffer (ACK buffer) at room temperature for 2min. Cells were blocked in the presence of Fc block (2.4G2; Leinco, C247) in magnetic-activated cell-sorting MACS buffer (0.5%BSA, 2mM EDTA in PBS) at 4°C. The following antibodies were used. Biolegend: CD45(30-F11), CD19(6D5), CD3(145–2C11), CD44(IM7), CD4 (PM4–5). BD: CD8 (53–6.7). Invitrogen: FOXP3(FJK-16s).

Microglia antigen presentation *in vitro* assay

C57BL/6-Tg (TcraTcrb) 1100Mb/J (OT-I) (Jax, #003831), B6.SJL-$Ptprc^a$ $Pepc^b$/BoyJ (B6. CD45.1) (Jax, #002014) were from Jackson laboratory. OT-1.CD45.1/2 mice were generated by crossing OT-1 and B6.CD45.1 for one generation. 8–12 week old mice were used for the experiment.

Author Manuscript Author Manuscript Author Manuscript Author Manuscript

To isolate APCs, spleens were chopped into small pieces and digested at 37°C for 45min with buffer containing 0.28U/ml Liberase TM (Roche, 5401119001), 100U/ml Hyaluronidase (Sigma, H3506), and 50U/ml DNase I (Roche, 10104159001) in RMPI1640 (Gibco, 11875093). Cells were pelleted down for CD11c microbeads (Miltenyi Biotec,130–125–835) enrichment based on manufacturer's instruction. DCs were sorted as $CD45^{+}CD11c^{+}MHC\text{-}II^{high}$ cells.

To enrich OT-1 CD8+ naïve T cells, Naïve CD8α^{+} T Cell Isolation Kit (Miltenyi Biotec, 130–096-543) were used for column-based enrichment. OT-1 naïve $CD8^{+}$ T cells were sorted followed by $CD45^{+}CD3^{+}CD8^{+}TCRV\beta5^{+}TCRV\alpha2^{+}CD62L^{+}CD44^{low}$ cells.

Microglia were sorted followed by $CD45^{low}CD11b^{+}$ cells after single cell collection from brain parenchyma with cortex and hippocampus. CellTrace Violet (5μM, Thermo Fisher, C34571) labeled 25,000 T cells were co-cultured with 20,000 microglia or DCs for 3 days in U-bottom 96-well plate (Corning, 07–200–720). A serial dilution of ovalbumin (Worthington, LS003049) starting from 1000μg/ml (2X dilution) was made and added into the wells. For microglia/OT-1 co-culture, two doses of IFNγ (100ng/ml and 1000ng/ml) were added at the same time. 3 days after, cells were analyzed by flow cytometry for T cell proliferation.

Flow cytometry and cell sorting were completed on a FACS CantoII or FACS AriaII instrument and analyzed using Flowjo (v10). Staining was performed at 4°C in the presence of Fc block (2.4G2; Leinco) in magnetic-activated cell-sorting (MACS) buffer (0.5%BSA, 2mM EDTA in PBS). The following antibodies were used. Biolegend: CD45 (30-F11), CD11b (M1/70), I-A/I-E (M5/114.15.2), CD3 (145–2C11), TCRVβ5 (MR9–4), TCRVα2 (B20.1), CD45.2 (104), CD45.1 (A20), CD44 (IM7), CD8α (53–6.7), CD62L (MEL-14).

Statistics

Statistical analysis was performed using Prism. Difference between groups were evaluated by Student's *t* test, one-way or two-way ANOVA followed by post hoc tests. For conditioned fear behavior, two-way ANOVA followed by Bonferroni test. Data expressed as mean ± s.e.m. *** $p<0.0001$, **$p<0.001$, *$p<0.05$, n.s. no significant difference.

Author Manuscript Author Manuscript Author Manuscript Author Manuscript

Extended Data

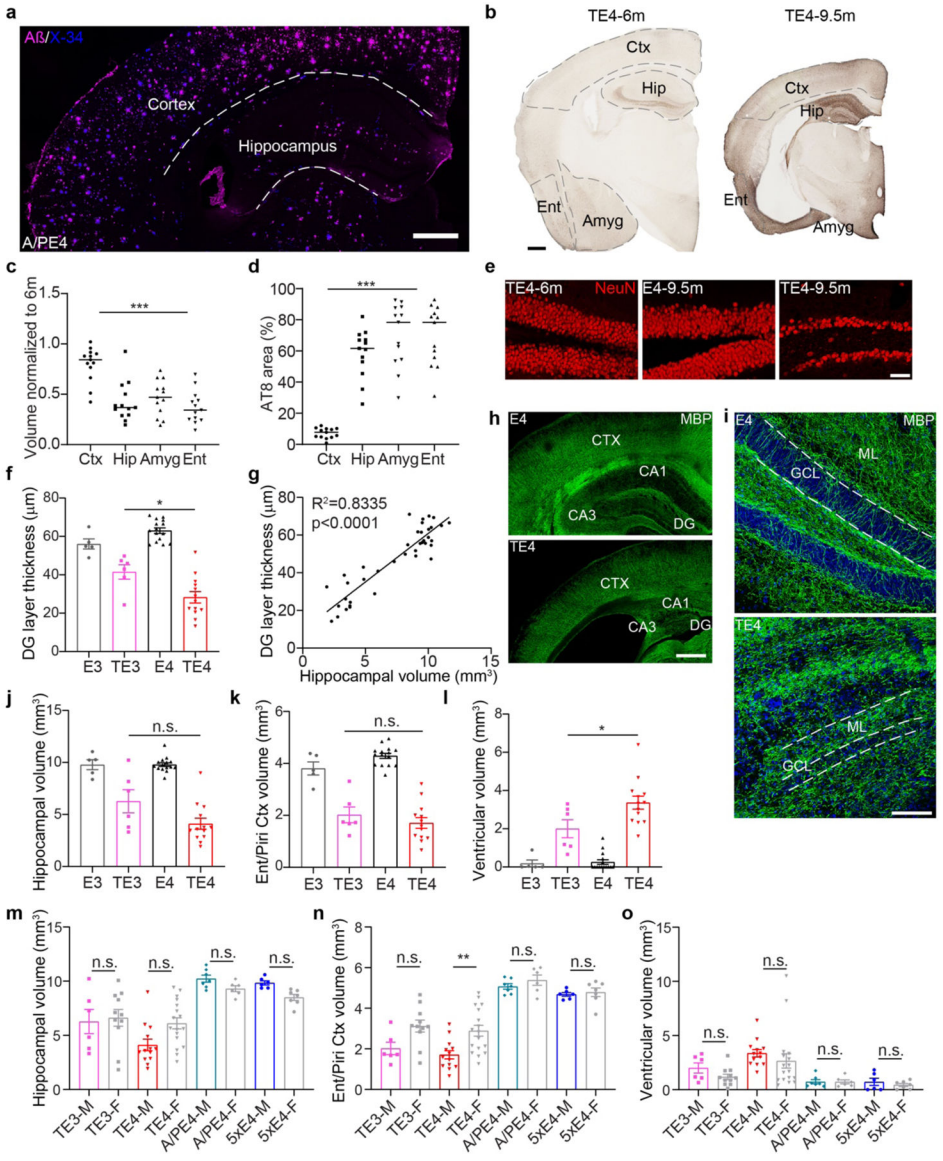

Extended Data Figure 1. ApoE4 exacerbates tau-mediated neurodegeneration

(**a**) Representative image of 9.5-month A/PE4 mouse brain sections stained with an anti-Aβ antibody and X-34. Scale bar=500μm. (**b**) Representative images of 6 and 9.5-month TE4 mouse brain sections stained with AT8 antibody. Scale bar=500μm. (**c**) Quantification of brain regional volumes of 9.5-month mice normalized to 6-month in b. TE4–6 months: n=7, TE4–9.5months: n=13. ***p<0.0001 for hippocampus (Hip) *vs.* cortex dorsal to the hippocampus (Ctx); amygdala (Amyg) *vs.* Ctx and entorhinal/piriform cortex (Ent) *vs.* Ctx. One-way ANOVA with Tukey's post hoc test. (**d**) Quantification of the area covered by AT8 of 9.5-month TE4 mouse brain sections in b. TE4–6 months: n=7, TE4–9.5months: n=13. ***p<0.0001 for Hip *vs.* Ctx; Amyg *vs.* Ctx and Ent *vs.* Ctx. One-way ANOVA with Tukey's post hoc test. (**e**) Representative images of 6-month TE4, 9.5-month E4, and 9.5-month TE4 mouse brain sections stained with NeuN. Scale bar=50 μm. (**f**) Thickness

Author Manuscript Author Manuscript Author Manuscript Author Manuscript

of granule cell layer of the dentate gyrus (DG) in 9.5-month E3, TE3, E4, TE4 mice. (E3: n=5, TE3: n=6, E4: n=15 and TE4: n=13). *p=0.0130 for TE3 *vs.* TE4. Two-way ANOVA with Tukey's post hoc test. (**g**) Correlation between DG neuronal layer thickness and hippocampal volume. n=39 biologically independent animals from f. Pearson correlation analysis. R^2=0.8335, p<0.0001. (**h**, **i**) Representative images of 9.5-month E4 and TE4 mouse brain sections stained with MBP. Scale bar=500μm in h. Scale bar=100μm in i. (**j-l**) Volumes of hippocampus, entorhinal/piriform cortex and posterior lateral ventricle in 9.5-month E3, TE3, E4, TE4 mice. (E3: n=5, TE3: n=6, E4: n=15 and TE4=13). p=0.0505 for TE3 *vs.* TE4 in comparing the volume of the hippocampus, *p=0.0207 for TE3 *vs.* TE4 in comparing the volume of the posterior lateral ventricle. Two-way ANOVA with Tukey's post hoc test. (**m-o**) Volumes of hippocampus, entorhinal/ piriform cortex and posterior lateral ventricle in 9.5-month TE3, TE4, A/PE4, 5xE4 male and female mice. (TE3-M: n=6, TE3-F: n=11, TE4-M: n=13, TE4-F: n=17, A/PE4-M: n=7, A/PE4-F: n=6, 5xE4-M: n=6, 5xE4-F: n=7). **p=0.0087 for TE4 male *vs.* female entorhinal/piriform cortex volume. Two-way ANOVA with Tukey's post hoc test. Data are mean ± s.e.m.

Author Manuscript Author Manuscript Author Manuscript Author Manuscript

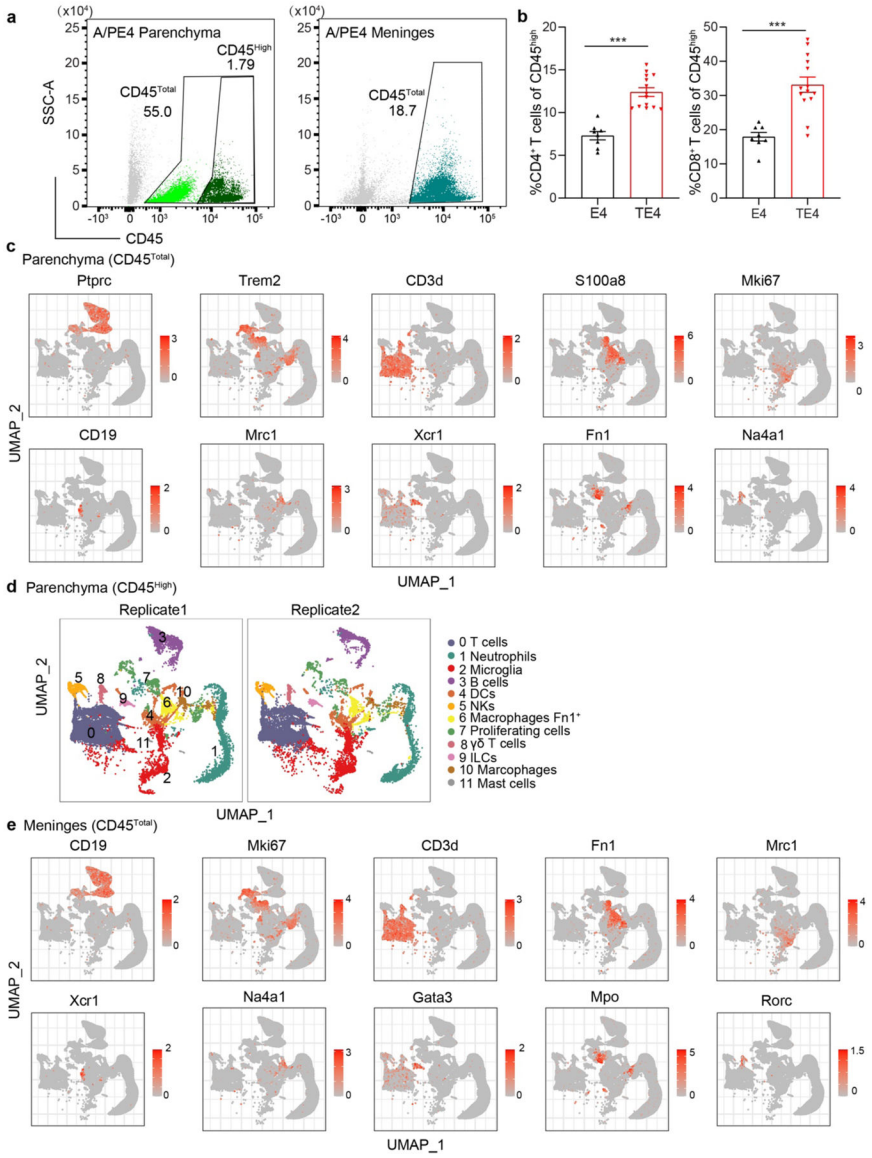

Extended Data Figure 2. Immune cell composition in brain parenchyma and meninges

(**a**) FACS sorting of CD45^{Total} and /or CD45^{high} cells from brain parenchyma and meninges from A/PE4 mice for single cell immune RNA-seq. (**b**) Analysis of the CD4 and CD8 positive T cells present in the brain of E4 and TE4 mice by flow cytometry. (E4: n=8, TE4: n=14) Data are mean ± s.e.m., ***p<0.0001, Unpaired two-tailed Student's *t* test. (**c**) Representative cell type specific makers in brain parenchyma (CD45^{Total}) clusters. (**d**) CD45^{high} immune cells from parenchyma assigned into 12 cell types as visualized by UMAP plot. (**e**) Representative cell type specific makers in meninges (CD45^{Total}).

Author Manuscript Author Manuscript Author Manuscript Author Manuscript

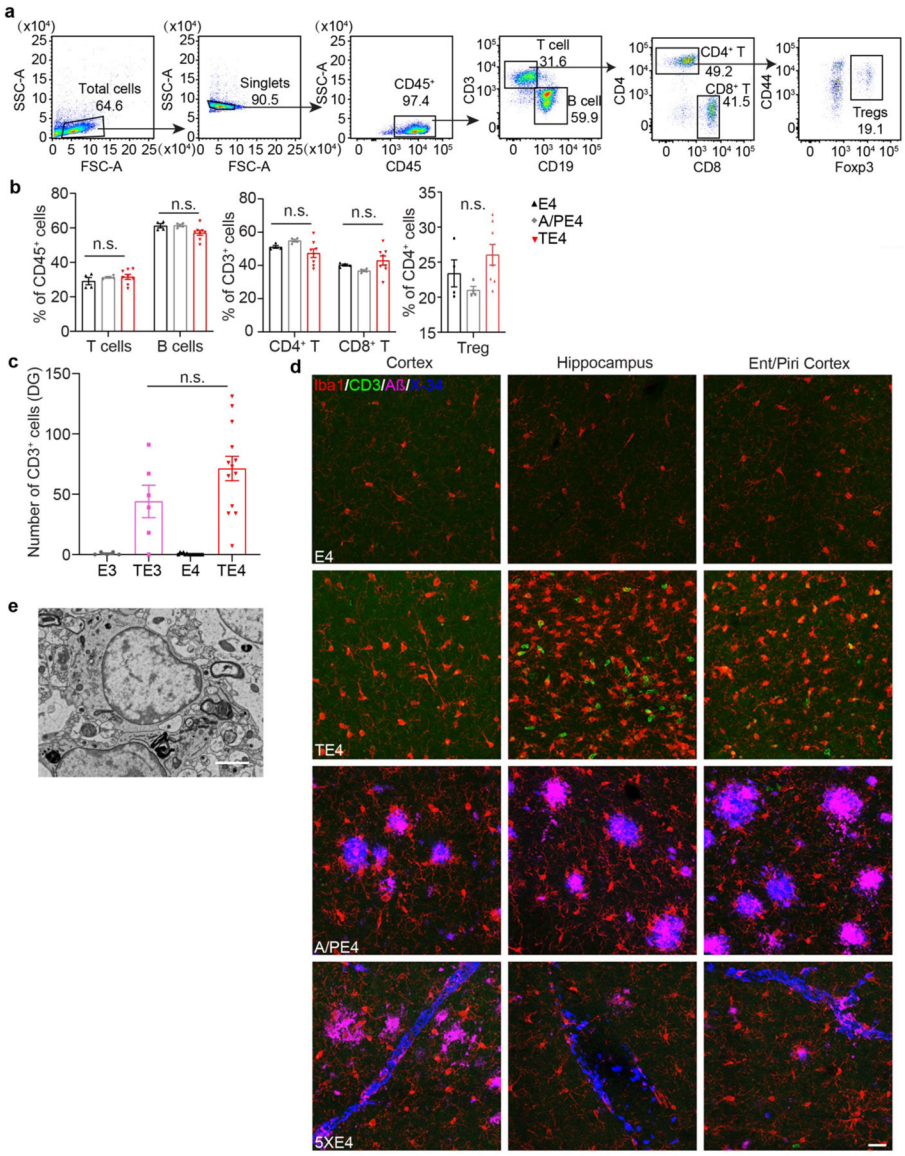

Extended Data Figure 3. T cell infiltration in the brain parenchyma with significant tauopathy

(**a**) Representative flow cytometry gating plot of splenic lymphocytes. (**b**) Quantification of the proportion of indicated lymphocytes and their subsets among 9.5-month E4, A/PE4, and TE4 mice. (E4: n=4, A/PE4: n=4, TE4: n=8). p=0.648, 0.492, 0.992 for E4 *vs.* A/PE4; E4 *vs.* TE4; A/PE4 *vs.* TE4 in T cells; p=0.614, 0.518, 0.089 for E4 *vs.* A/PE4; E4 *vs.* TE4; A/PE4 *vs.* TE4 in $CD4^+$ T cells; p=0.665, 0.719, 0.196 for E4 *vs.* A/PE4; E4 *vs.* TE4; A/PE4 *vs.* TE4 in $CD8^+$ T cells. Two-way ANOVA with Tukey's post hoc test. p=0.629, 0.472, 0.095 for E4 *vs.* A/PE4; E4 *vs.* TE4; A/PE4 *vs.* TE4 in Treg. One-way ANOVA with Tukey's post hoc test. (**c**) Quantification of $CD3^+$ T cell number per DG area with $0.3mm^2$ in 9.5 month E3, TE3, E4, TE4 mice. (E3: n=5, TE3: n=6, E4: n=15 and TE4: n=13). Two-way ANOVA with Tukey's post hoc test. p=0.1342 for TE3 *vs.* TE4. (**d**) Representative images of 9.5-month old E4, TE4, A/PE4 and 5xE4 mouse brain sections stained with CD3, Iba1, Aβ and X-34. Scale bar=20μm. Images are representative of results from n=4 in E4,

A/PE4 and TE4 respectively. (**e**) TEM image demonstrating presence of a cell with T cell like features in brain parenchyma of 9.5 month of TE4 mouse. Scale bar=2μm. Images are representative of results from n=3 in TE4 mice.

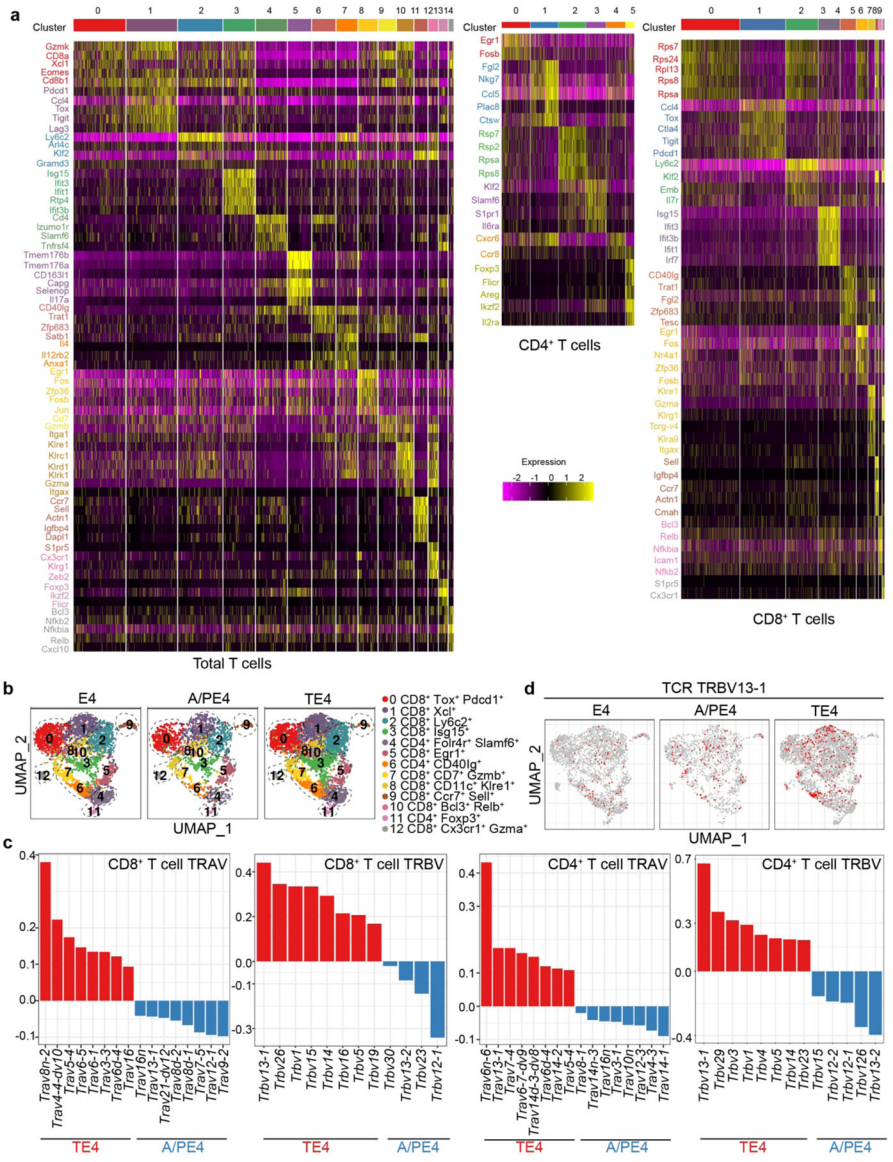

Extended Data Figure 4. Characterization of T cell populations within the parenchyma and meninges of mice with amyloid or tau pathology

(**a**) Heatmap showing identified marker genes in each of the categorized cell types in Total T cells, CD4$^+$ and CD8$^+$ T cells. (**b**) Total T cells from brain parenchyma and meninges with TCR assigned into 13 cell types as visualized by UMAP plot. (**c**) TRAV and TRBV enrichment in CD8$^+$ and CD4$^+$ T cells in TE4 and A/PE4 mice. (**d**) Representative TCR-TRBV projection in E4, A/PE4 and TE4 mice.

Author Manuscript Author Manuscript Author Manuscript Author Manuscript

Author Manuscript Author Manuscript Author Manuscript Author Manuscript

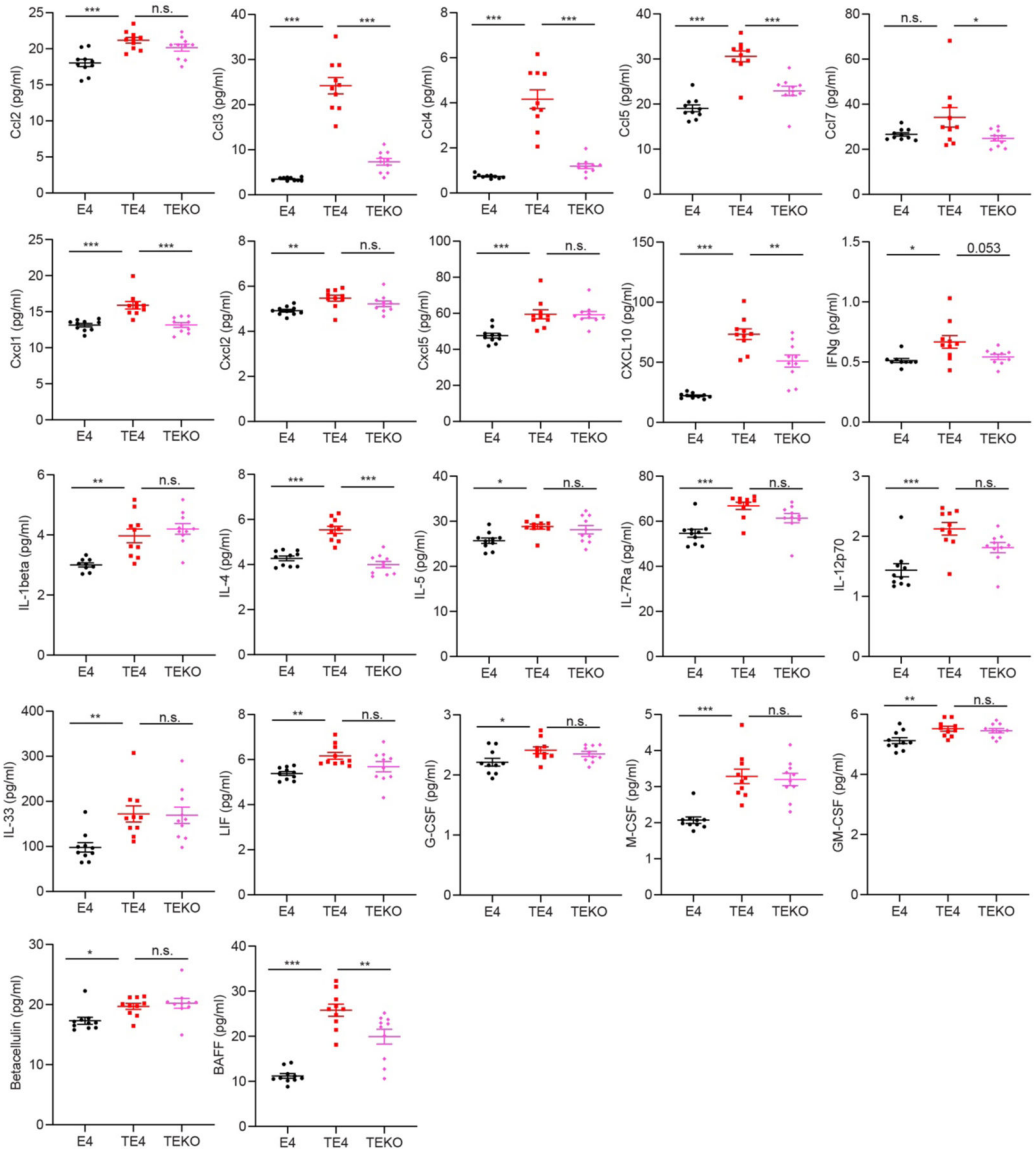

Extended Data Figure 5. Expression of cytokines, chemokines, growth factors and soluble receptors in brain lysates

Quantification of cytokines, chemokines, growth factors and soluble receptors in brain lysates in 9.5 month old E4, TE4, and TEKO mice. (E4: n=10, TE4: n=10 and TEKO: n=10). One-way ANOVA with Tukey's post hoc test. With Q=0.1% identify outlier function, n=1 E4 and n=1 TEKO samples for IFN-γ measurements were removed; n=1 E4 sample for IL-1β measurements was removed. ***p=0.0001, ***p<0.0001, ***p<0.0001, ***p<0.0001, p=0.1261, ***p<0.0001, **p=0.0038, ***p=0.0005, ***p<0.0001, *p=0.0144, **p=0.0022, ***p<0.0001, *p=0.0126, ***p=0.0002, ***p=0.0001, **p=0.0074, **p=0.0059, *p=0.0434, ***p<0.0001, **p=0.007, *p=0.038, ***p<0.0001 for E4 *vs.*TE4 following the panel order. p=0.2757, ***p<0.0001, ***p<0.0001, ***p<0.0001, *p=0.489, ***p<0.0001, p=0.2539, p=0.9952, **p=0.0011, p=0.053, n=0.625, ***p<0.0001, n=0.7867, p=0.1013, p=0.087, p=0.9905, p=0.1107,

Author Manuscript Author Manuscript Author Manuscript Author Manuscript

p=0.7159, p=0.9193, p=0.8426, p=0.83, **p=0.0076 for TE4 *vs.* TEKO following the panel order. Data are mean ± s.e.m.; One-way ANOVA with Tukey's post hoc test.

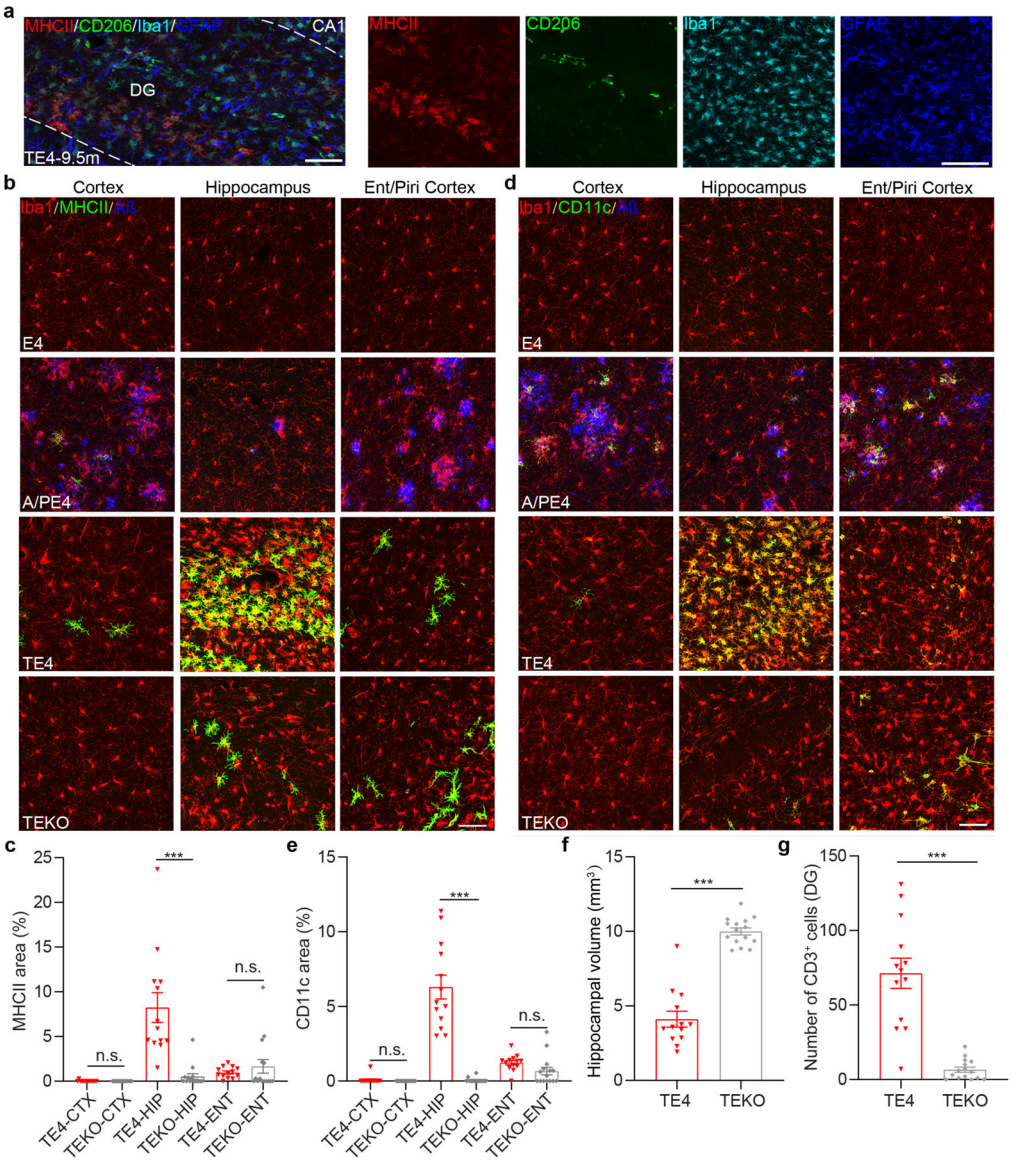

Extended Data Figure 6. Changes in microglia and T cells with Tau-meditated neurodegeneration require ApoE

(**a**) MHCII, CD206, Iba1 and GFAP staining in 9.5-month TE4 mice. Scale bar=100μm. Images are representative of results from n=13 in TE4 mice. (**b**) Iba1, MHCII and Aβ staining in 9.5 month E4, A/PE4, TE4 and TEKO mice in Cortex dorsal to Hippocampus, Hippocampus and Ent/Piri cortex. Scale bar=50μm. (**c**) Quantification of the area covered by MHCII in Ctx, Hip and Ent in 9.5-month TE4 and TEKO mice. (TE4: n=13 and TEKO: n=15). ***p<0.0001 for TE4-Hip *vs.* TEKO-Hip. One-way ANOVA with Tukey's post hoc test. (**d**) Iba1, CD11c and Aβ staining in 9.5-month E4, A/PE4, TE4 and TEKO mice in Prefrontal cortex, Hippocampus and Ent/Piri cortex. Scale bar=50μm. (**e**) Quantification of the area covered by CD11c in Ctx, Hip and Ent in 9.5-month TE4 and TEKO mice.

(TE4: n=13 and TEKO: n=15). ***p<0.0001 for TE4-Hip *vs.* TEKO-Hip. One-way ANOVA with Tukey's post hoc test. (**f**) Volume of hippocampus in 9.5-month TE4 and TEKO mice. (TE4: n=13 and TEKO: n=15). ***p<0.0001. Unpaired two-tailed Student's *t* test. (**g**) Quantification of numbers of $CD3^+$ T cells in DG per $0.3mm^2$. (TE4: n=13 and TEKO: n=15). ***p<0.0001. Data are mean ± s.e.m.; Unpaired two-tailed Student's *t* test.

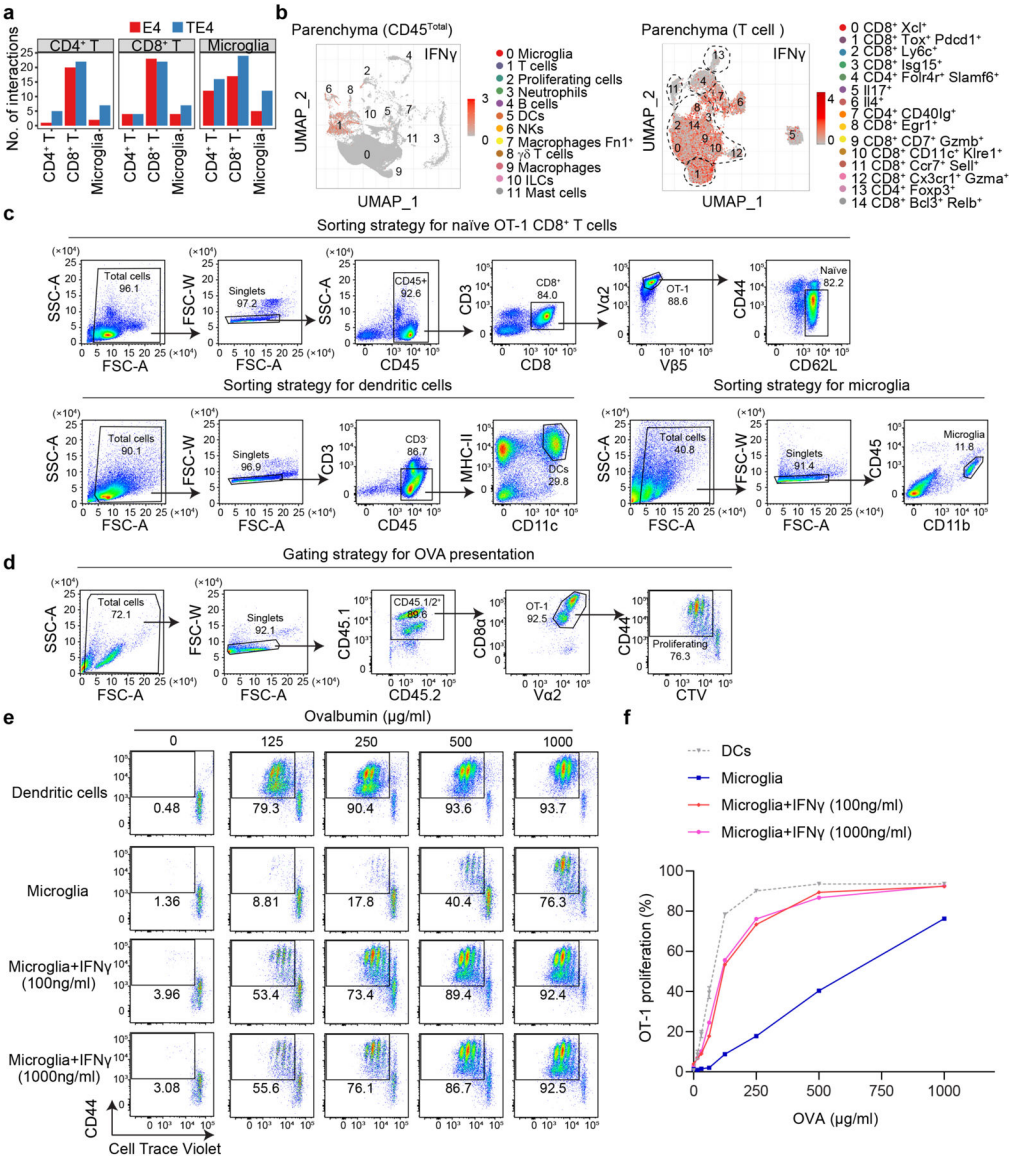

Extended Data Figure 7. IFN-γ in the T cell population and microglia can directly present antigen to $CD8^+$ T cells *in vitro*

(**a**) Ligand-receptor analysis in T cells and microglia. (**b**) IFN-γ expression in brain parenchyma ($CD45^{Total}$) 12 cell types and T cells from brain parenchyma 15 clusters of T cells as visualized by UMAP plot. (**c**) The gating strategy for sorting naïve OT-1 $CD8^+$ T cells, dendritic cells (DCs), and microglia. (**d**) Representative flow cytometry plot to assess the proliferation of OT-1 T cells by cell tracer violet (CTV) dilution after 3 days of co-culture with APCs in the presence of OVA. (**e**) Representative flow cytometry plot

Author Manuscript Author Manuscript Author Manuscript Author Manuscript

showing dose dependent OVA antigen presentation by DCs, microglia, or microglia in the presence of IFNγ assayed by OT-1 proliferation. (**f**) Percent of proliferating OT-1 T cells under the indicated conditions. Data are from one representative experiment. Two independent experiments were done showing similar results.

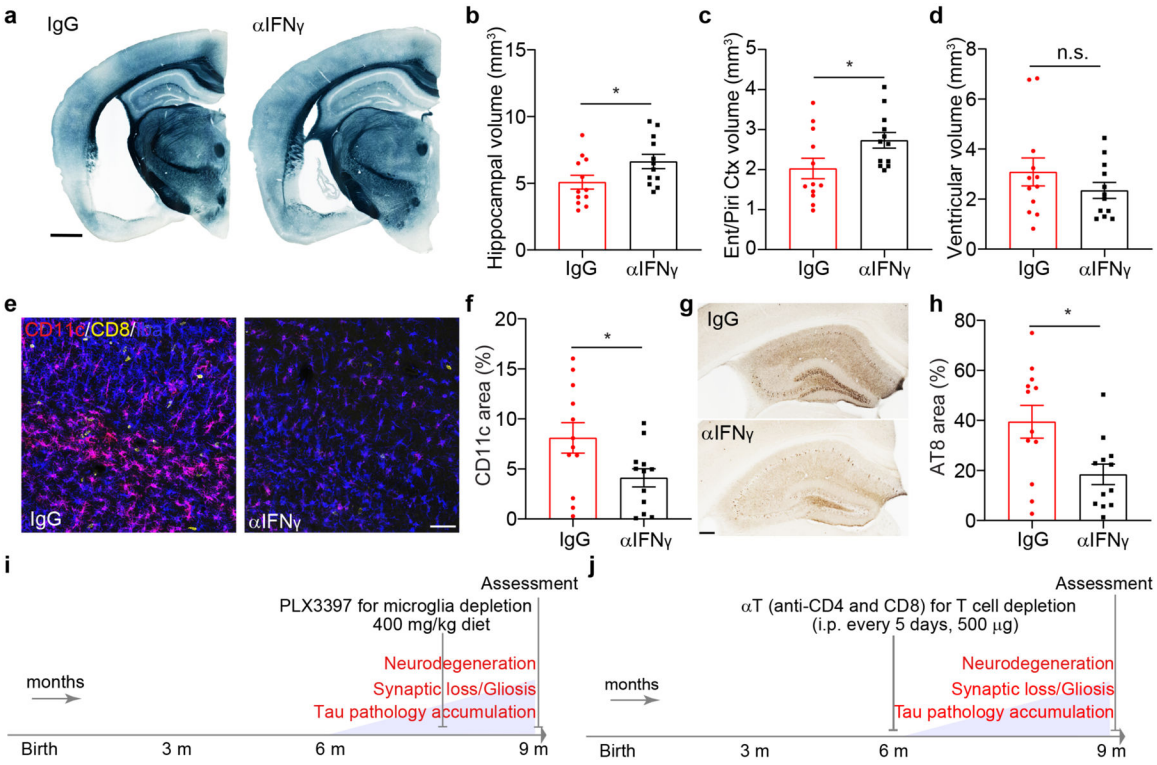

Extended Data Figure 8. Blocking IFNγ signaling reduces tau-mediated neurodegeneration and tau pathology

(a) Representative images of 9.5-month TE3-IgG and TE3-αIFN-γ treated mouse brain sections stained with Sudan black. Scale bar=1mm. (b-d) Volumes of hippocampus, entorhinal/piriform cortex and posterior lateral ventricle in 9.5-month TE3-IgG and TE3-αIFNγ treated mice. (TE3-IgG: n=12 and TE3-αIFNγ: n=12). p=0.0479, 0.0398, 0.265 for TE3-IgG *vs.* TE3-αIFNγ in comparing the volumes of hippocampus, entorhinal/piriform cortex and posterior lateral ventricle, respectively. Unpaired two-tailed Student's t test. (e) CD11c, CD8, Iba1 staining in 9.5-month TE3-IgG and TE3-αIFNγ treated mice. Scale bar=50μm. (f) Quantification of area covered by CD11c in 9.5-month TE3-IgG and TE3-αIFNγ mice. (TE3-IgG: n=12 and TE3-αIFNγ: n=12). *p=0.0344. Unpaired two-tailed Student's t test. (g) Representative images of 9.5-month TE3-IgG and TE3-αIFNγ treated mouse brain sections stained with AT8 antibody. Scale bar=250μm. (h) p-Tau (AT8) covered area in 9.5-month TE3-IgG and TE3-αIFNγ treated mice. (TE3-IgG: n=12 and TE3-αIFNγ: n=12). *p=0.0122. Unpaired two-tailed Student's t test. (i) Schematic representation of the timeline of PLX3397 treatment for microglia depletion. (j) Schematic representation of the timeline of anti-CD4 and anti-CD8 antibody treatment for T cell depletion.

Author Manuscript Author Manuscript Author Manuscript Author Manuscript

Author Manuscript Author Manuscript Author Manuscript Author Manuscript

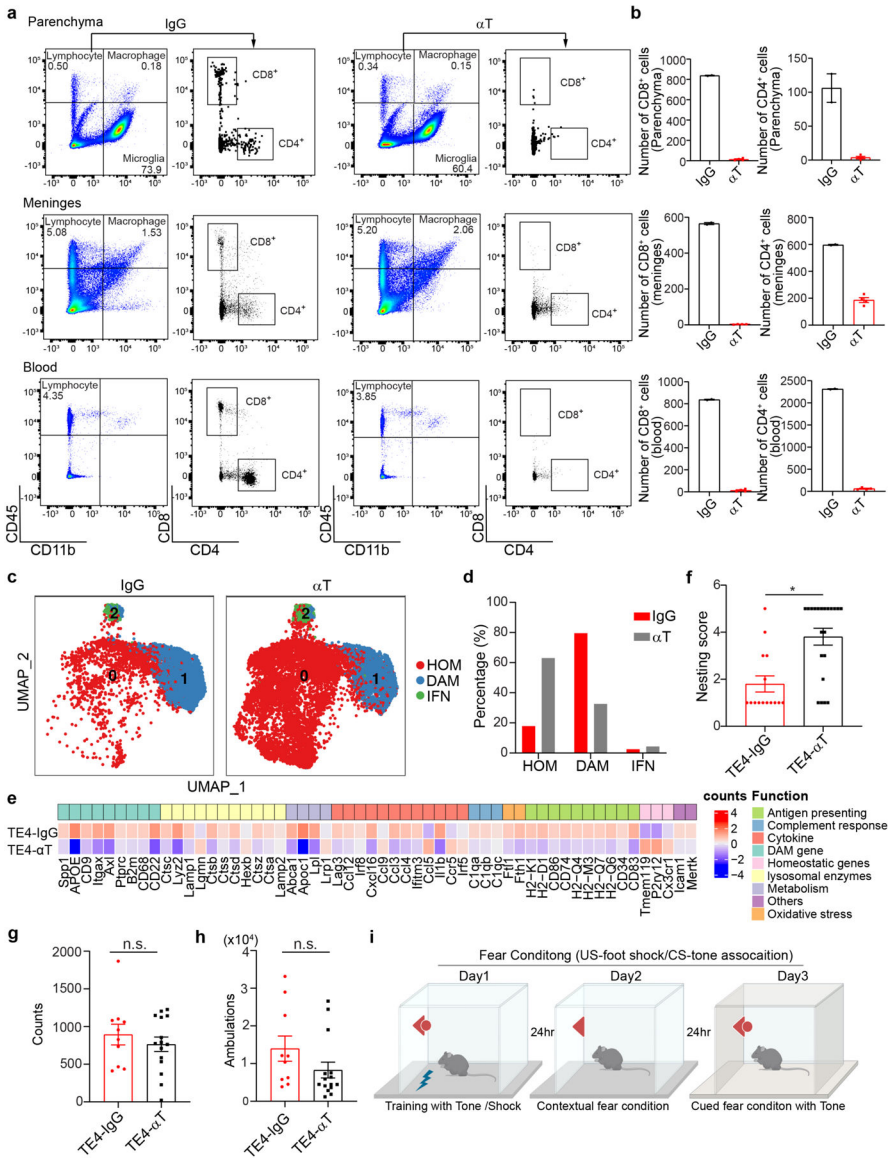

Extended Data Figure 9. T cell depletion in tauopathy mice

(**a**) Representative flow cytometry gating plot and quantification of CD4$^+$, CD8$^+$ T cells in brain parenchyma, meninges and blood in IgG control or α-CD4 and α-CD8 (αT) treated mice. (**b**) Bar plot showing the number of CD8$^+$ T and CD4$^+$ T cells in IgG and αT treated mice. (IgG: n=2 and αT: n=4). Data are mean ± s.e.m. (**c**) Microglia from brain parenchyma of TE4-IgG and TE4-αT treated mice assigned into 3 categories as visualized by UMAP plot. (**d**) Bar plot showing the percentage of the 3 categories of microglia in TE4-IgG and TE4-αT mice. (**e**) Heat map showing representative functional genes specifically expressed in active microglia clusters in TE4-IgG and TE4-αT mice. (**f**) Quantification of nest-building behavior at 9.5 months age. (TE4-IgG: n=15 and TE4-αT: n=21). *p=0.02 for IgG *vs.* αT. Fisher's exact test. (**g**) Quantification of total rearing at baseline levels of general exploratory behavior in 1 h. (TE4-IgG: n=10 and TE4-αT: n=15). p=0.4363 for TE4-IgG *vs.* TE4-αT. Unpaired two-tailed Student's *t* test. (**h**) Quantification of total

ambulations at baseline levels of locomotor activity levels in 1 h. (TE4-IgG: n=10 and TE4-αT: n=15). p=0.0709. Two-tailed Mann-Whitney test. (**i**) Schematic representation of fear conditioning behavioral paradigms.

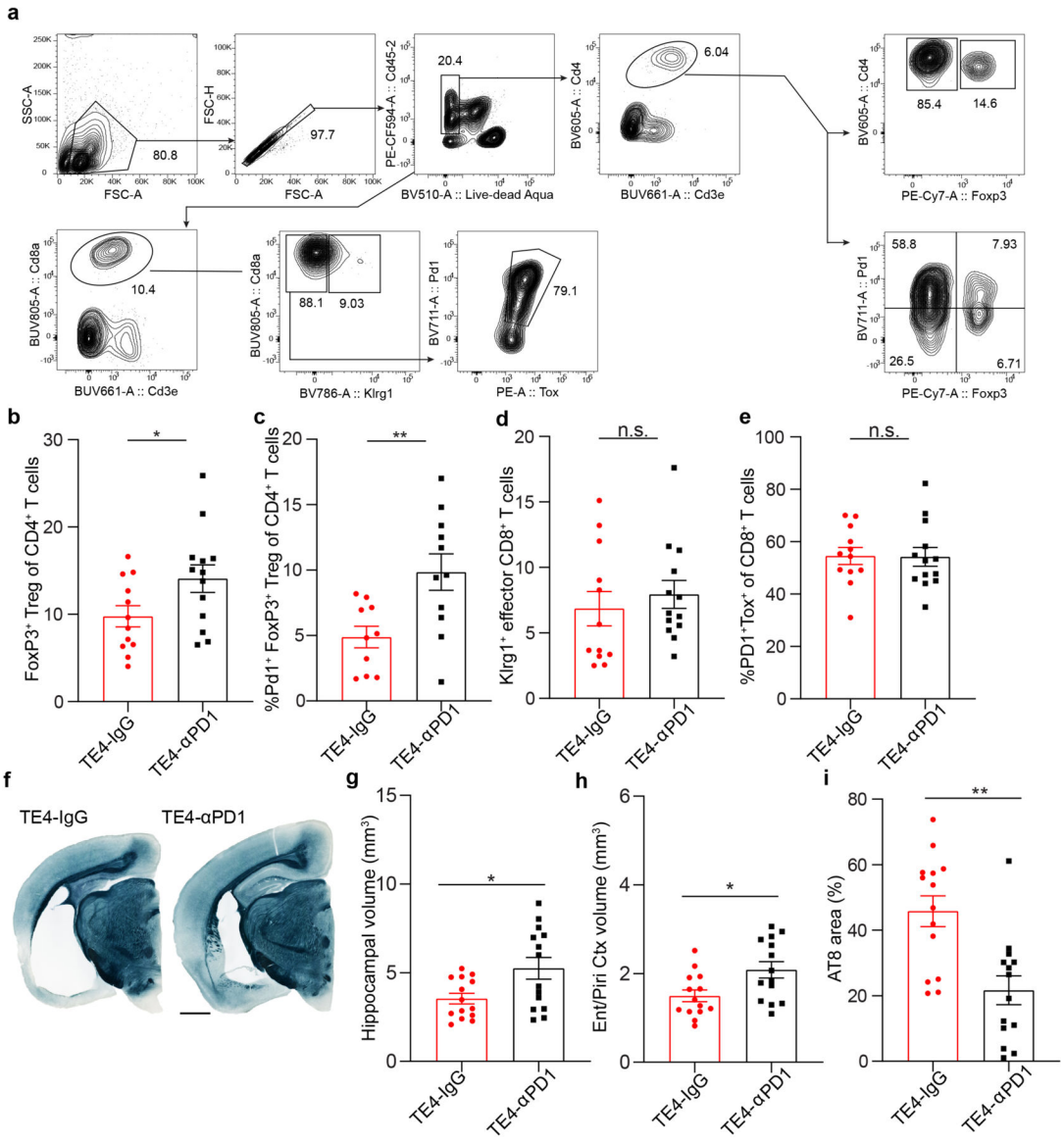

Extended Data Figure 10. Blocking PD-1 immune checkpoint increases Foxp3$^+$CD4$^+$ Tregs and reduces tau-mediated neurodegeneration

(**a**) The gating strategy for sorting Foxp3$^+$ CD4$^+$ Treg, Pd1$^+$ Foxp3$^+$ CD4$^+$ Treg, Klrg1$^+$ effector CD8$^+$ T cells, PD-1$^+$ Tox1$^+$ CD8$^+$ exhausted T cells in the brain parenchyma. (**b-e**) Quantification of T cell populations in the brain parenchyma of mice acutely treated with IgG control and αPD-1 antibodies. (TE4-IgG: n=12 and TE4-αPD-1: n=13 for b, d, e; TE4-IgG: n=10 and TE4-αPD-1: n=11 for c). *p=0.041, **p=0.0075, p=0.52, p=0.945 for Foxp3$^+$CD4$^+$ Treg, Pd1$^+$ Foxp3$^+$ CD4$^+$ Treg, Klrg1$^+$ effector CD8$^+$ T cells, PD-1$^+$ Tox1$^+$ CD8$^+$ exhausted T cells. Unpaired two-tailed Student's *t* test. (**f**) Representative images of 9.5-month TE4-IgG and TE4-αPD-1 treated mouse brain sections stained with

Author Manuscript Author Manuscript Author Manuscript Author Manuscript

Author Manuscript Author Manuscript Author Manuscript Author Manuscript

Sudan black. Scale bar=1mm. (**g-h**) Volumes of hippocampus, entorhinal/piriform cortex in 9.5-month TE4-IgG and TE4-αPD-1 treated mice. (TE4-IgG: n=14 and TE4-αPD-1: n=14). *p=0.018 and 0.015 for TE4-IgG *vs.* TE4-αPD-1 in comparing the volumes of hippocampus, entorhinal/piriform cortex, respectively. Unpaired two-tailed Student's *t* test. (**i**) Quantification of the area covered by AT8 in DG per slice in 9.5-month TE4-IgG *vs.* TE4-αPD-1 mice (TE4-IgG: n=14 and TE4-αPD: n=14). **p=0.0009. Unpaired two-tailed Student's *t* test.

Extended Data Table 1.

Single cell immune sequencing sample information

ID	Age (months)	Sex	Genetics	Genetic background	Brain regions for sequencing	Total cell number	Microglia cell number	Median genes per microglia	T cell number	Median genes per T cell	Number of Mice
1	9.5	M	E4-Replicate1	BL6	CD45Total Cortex and Hippocampus	22248	20547	2091	489	2044	10
2	9.5	M	E4-Replicate2	BL6	CD45Total Cortex and Hippocampus	4640	4107	1466	198	1762	5
3	9.5	M	A/PE4	BL6	CD45Total Cortex and Hippocampus	9869	9216	2019	263	3044	5
4	9.5	M	TE4-Replicate1	BL6	CD45Total Cortex and Hippocampus	8570	7210	2913	745	2111	5
5	9.5	M	TE4-Replicate2	BL6	CD45Total Cortex and Hippocampus	6305	4915	1470	700	1782	5
6	9.5	M	E4-Replicate1	BL6	CD45high Cortex and Hippocampus	9489	501	2158	3396	1897	10
7	9.5	M	E4-Replicate2	BL6	CD45high Cortex and Hippocampus	6019	544	2029	2251	1498	5
8	9.5	M	A/PE4	BL6	CD45high Cortex and Hippocampus	7161	1352	2822	2300	1748	5
9	9.5	M	TE4-Replciate1	BL6	CD45high Cortex and Hippocampus	6741	292	2060	4587	2352	5
10	9.5	M	TE4-Replicate2	BL6	CD45high Cortex and Hippocampus	11364	1765	2322	5602	1740	5
11	9.5	M	E4-Replicate1	BL6	CD45Total Meninges	27042	950	1718	1600	1708	10
12	9.5	M	E4-Replicate2	BL6	CD45Total Meninges	13554	1358	2030	1279	1298	5
13	9.5	M	A/PE4	BL6	CD45Total Meninges	11197	593	1786	468	1517	5
14	9.5	M	TE4-Replicate1	BL6	CD45Total Meninges	14314	80	2886	1497	1953	5
15	9.5	M	TE4-Replicate2	BL6	CD45Total Meninges	10741	653	1658	1053	1380	5

Author Manuscript Author Manuscript Author Manuscript Author Manuscript

ID	Age (months)	Sex	Genetics	Genetic background	Brain regions for sequencing	Total cell number	Microglia cell number	Median genes per microglia	T cell number	Median genes per T cell	Number of Mice
16	9.5	M	TE4-Ctrl (IgG)	BL6	CD45Total Cortex and Hippocampus	12572	11310	2068	335	1779	5
17	9.5	M	TE4-αT	BL6	CD45Total Cortex and Hippocampus	15080	14009	1974	74	1605	5

Extended Data Table 2.

Alzheimer's disease patient sample information

ID	Age	Sex	ApoE isoform	Braak Score	Postmortem interval (PMI)
1	70	F	E4/E4	I	2
2	78	M	E2/E2	I	1.66
3	81	F	E4/E4	II	3
4	80	F	E4/E4	VI	1.33
5	68	F	E2/E2	VI	3.08
6	80	M	E3/E3	VI	2.16
7	83	M	E4/E4	VI	2.83
8	89	F	E3/E3	VI	2.7
9	90	F	E3/E3	VI	2.53
10	89	F	E4/E4	VI	2.5

Extended Data Table 3.

Immune cell number of each cluster in brain parenchyma and meninges

$CD45^{Total}$ immune cell number per cluster in brain parenchyma (Fig. 1f)

Cluster	Genotype	Replica	Total cell number	Cell number/Cluster	Percentage (%)
0 Microglia	E4	Rep1	22248	20547	92.4
0 Microglia	E4	Rep2	4640	4107	88.5
0 Microglia	A/PE4	Rep1	9869	9216	93.4
0 Microglia	TE4	Rep1	8570	7210	84.1
0 Microglia	TE4	Rep2	6305	4915	78.0
1 T cells	E4	Rep1	22248	489	2.2
1 T cells	E4	Rep2	4640	198	4.3
1 T cells	A/PE4	Rep1	9869	263	2.7
1 T cells	TE4	Rep1	8570	745	8.7
1 T cells	TE4	Rep2	6305	700	11.1
2 Proliferating cells	E4	Rep1	22248	226	1.0
2 Proliferating cells	E4	Rep2	4640	74	1.6

Author Manuscript Author Manuscript Author Manuscript Author Manuscript

Cluster	Genotype	Replica	Total cell number	Cell number/Cluster	Percentage (%)
2 Proliferating cells	A/PE4	Rep1	9869	145	1.5
2 Proliferating cells	TE4	Rep1	8570	114	1.3
2 Proliferating cells	TE4	Rep2	6305	244	3.9
3 Neutrophils	E4	Rep1	22248	349	1.6
3 Neutrophils	E4	Rep2	4640	54	1.2
3 Neutrophils	A/PE4	Rep1	9869	101	1.0
3 Neutrophils	TE4	Rep1	8570	118	1.4
3 Neutrophils	TE4	Rep2	6305	149	2.4
4 B cells	E4	Rep1	22248	207	0.9
4 B cells	E4	Rep2	4640	84	1.8
4 B cells	A/PE4	Rep1	9869	32	0.3
4 B cells	TE4	Rep1	8570	64	0.7
4 B cells	TE4	Rep2	6305	57	0.9
5 DCs	E4	Rep1	22248	126	0.6
5 DCs	E4	Rep2	4640	37	0.8
5 DCs	A/PE4	Rep1	9869	28	0.3
5 DCs	TE4	Rep1	8570	93	1.1
5 DCs	TE4	Rep2	6305	116	1.8
6 NKs	E4	Rep1	22248	97	0.4
6 NKs	E4	Rep2	4640	21	0.5
6 NKs	A/PE4	Rep1	9869	14	0.1
6 NKs	TE4	Rep1	8570	76	0.9
6 NKs	TE4	Rep2	6305	55	0.9
7 Macrophages Fn1+	E4	Rep1	22248	92	0.4
7 Macrophages $Fn1^{+}$	E4	Rep2	4640	19	0.4
7 Macrophages $Fn1^{+}$	A/PE4	Rep1	9869	14	0.1
7 Macrophages $Fn1^{+}$	TE4	Rep1	8570	37	0.4
7 Macrophages $Fn1^{+}$	TE4	Rep2	6305	20	0.3
8 γδ T cells	E4	Rep1	22248	19	0.1
8 γδ T cells	E4	Rep2	4640	18	0.4
8 γδ T cells	A/PE4	Rep1	9869	26	0.3
8 γδ T cells	TE4	Rep1	8570	54	0.6
8 γδ T cells	TE4	Rep2	6305	34	0.5
9 Macrophages	E4	Rep1	22248	57	0.3
9 Macrophages	E4	Rep2	4640	19	0.4
9 Macrophages	A/PE4	Rep1	9869	22	0.2
9 Macrophages	TE4	Rep1	8570	31	0.4
9 Macrophages	TE4	Rep2	6305	5	0.1
10 ILCs	E4	Rep1	22248	33	0.1

Author Manuscript Author Manuscript Author Manuscript Author Manuscript

Cluster	Genotype	Replica	Total cell number	Cell number/Cluster	Percentage (%)
10 ILCs	E4	Rep2	4640	4	0.1
10 ILCs	A/PE4	Rep1	9869	7	0.1
10 ILCs	TE4	Rep1	8570	24	0.3
10 ILCs	TE4	Rep2	6305	9	0.1
11 Mast cells	E4	Rep1	22248	6	0.0
11 Mast cells	E4	Rep2	4640	5	0.1
11 Mast cells	A/PE4	Rep1	9869	1	0.0
11 Mast cells	TE4	Rep1	8570	4	0.0
11 Mast cells	TE4	Rep2	6305	1	0.0

$CD45^{Total}$ immune cell number per cluster in meninges (Fig. 1h)

Cluster	Genotype	Replica	Total cell number	Cell number/Cluster	Percentage (%)
0 Neutrophils	E4	Rep1	27042	10165	37.6
0 Neutrophils	E4	Rep2	13554	5061	37.3
0 Neutrophils	A/PE4	Rep1	11197	3963	35.4
0 Neutrophils	TE4	Rep1	14314	5923	41.4
0 Neutrophils	TE4	Rep2	10741	4059	37.8
1 B cells	E4	Rep1	27042	6590	24.4
1 B cells	E4	Rep2	13554	1632	12.0
1 B cells	A/PE4	Rep1	11197	3237	28.9
1 B cells	TE4	Rep1	14314	2394	16.7
1 B cells	TE4	Rep2	10741	1977	18.4
2 Proliferating cells	E4	Rep1	27042	3392	12.5
2 Proliferating cells	E4	Rep2	13554	1327	9.8
2 Proliferating cells	A/PE4	Rep1	11197	1336	11.9
2 Proliferating cells	TE4	Rep1	14314	1337	9.3
2 Proliferating cells	TE4	Rep2	10741	1252	11.7
3 T cells	E4	Rep1	27042	1600	5.9
3 T cells	E4	Rep2	13554	1279	9.4
3 T cells	A/PE4	Rep1	11197	468	4.2
3 T cells	TE4	Rep1	14314	1497	10.5
3 T cells	TE4	Rep2	10741	1053	9.8
4 Macrophages $Fn1^{+}$	E4	Rep1	27042	1701	6.3
4 Macrophages $Fn1^{+}$	E4	Rep2	13554	916	6.8
4 Macrophages $Fn1^{+}$	A/PE4	Rep1	11197	635	5.7
4 Macrophages $Fn1^{+}$	TE4	Rep1	14314	959	6.7
4 Macrophages $Fn1^{+}$	TE4	Rep2	10741	570	5.3
5 DCs	E4	Rep1	27042	1308	4.8

Author Manuscript Author Manuscript Author Manuscript Author Manuscript

Cluster	Genotype	Replica	Total cell number	Cell number/Cluster	Percentage (%)
5 DCs	E4	Rep2	13554	997	7.4
5 DCs	A/PE4	Rep1	11197	574	5.1
5 DCs	TE4	Rep1	14314	1132	7.9
5 DCs	TE4	Rep2	10741	518	4.8
6 Microglia	E4	Rep1	27042	950	3.5
6 Microglia	E4	Rep2	13554	1358	10.0
6 Microglia	A/PE4	Rep1	11197	593	5.3
6 Microglia	TE4	Rep1	14314	80	0.6
6 Microglia	TE4	Rep2	10741	653	6.1
7 NKs	E4	Rep1	27042	427	1.6
7 NKs	E4	Rep2	13554	307	2.3
7 NKs	A/PE4	Rep1	11197	122	1.1
7 NKs	TE4	Rep1	14314	385	2.7
7 NKs	TE4	Rep2	10741	197	1.8
8 Macrophages	E4	Rep1	27042	489	1.8
8 Macrophages	E4	Rep2	13554	299	2.2
8 Macrophages	A/PE4	Rep1	11197	107	1.0
8 Macrophages	TE4	Rep1	14314	293	2.0
8 Macrophages	TE4	Rep2	10741	232	2.2
9 ILCs	E4	Rep1	27042	240	0.9
9 ILCs	E4	Rep2	13554	176	1.3
9 ILCs	A/PE4	Rep1	11197	96	0.9
9 ILCs	TE4	Rep1	14314	159	1.1
9 ILCs	TE4	Rep2	10741	104	1.0
10 Mast cells	E4	Rep1	27042	134	0.5
10 Mast cells	E4	Rep2	13554	95	0.7
10 Mast cells	A/PE4	Rep1	11197	48	0.4
10 Mast cells	TE4	Rep1	14314	82	0.6
10 Mast cells	TE4	Rep2	10741	77	0.7
11 γδ T cells	E4	Rep1	27042	46	0.2
11 γδ T cells	E4	Rep2	13554	107	0.8
11 γδ T cells	A/PE4	Rep1	11197	18	0.2
11 γδ T cells	TE4	Rep1	14314	73	0.5
11 γδ T cells	TE4	Rep2	10741	49	0.5

T cell number per cluster in brain parenchyma and meninges (Fig. 3b)

Cluster	Region	Total cell number	Cell number/Cluster	Percentage (%)
0 $CD8^{+}Xcl1^{+}$	Parenchyma	18565	3594	19.4

Author Manuscript Author Manuscript Author Manuscript Author Manuscript

Cluster	Region	Total cell number	Cell number/Cluster	Percentage (%)
0 $CD8^+Xcl1^+$	meninges	5040	457	9.1
1 $CD8^+Tox^+Pdcd1^+$	Parenchyma	18565	2607	14.0
1 $CD8^+Tox^+Pdcd1^+$	meninges	5040	537	10.7
2 $CD8^+Ly6c^+$	Parenchyma	18565	2422	13.0
2 $CD8^+Ly6c^+$	meninges	5040	548	10.9
3 $CD8^+Isg15^+$	Parenchyma	18565	1635	8.8
3 $CD8^+Isg15^+$	meninges	5040	303	6.0
4 $CD4^+Folr4^+Slamf6^+$	Parenchyma	18565	1096	5.9
4 $CD4^+Folr4^+Slamf6^+$	meninges	5040	724	14.4
5 $Il17^+$	Parenchyma	18565	1283	6.9
5 $Il17^+$	meninges	5040	302	6.0
6 $Il4^+$	Parenchyma	18565	1112	6.0
6 $Il4^+$	meninges	5040	274	5.4
7 $Cd4^+Cd40lg^+$	Parenchyma	18565	923	5.0
7 $Cd4^+Cd40lg^+$	meninges	5040	341	6.8
8 $Cd8^+Egr1^+$	Parenchyma	18565	992	5.3
8 $Cd8^+Egr1^+$	meninges	5040	13	0.3
9 $Cd8^+Cd7^+Gzmb^+$	Parenchyma	18565	1003	5.4
9 $Cd8^+Cd7^+Gzmb^+$	meninges	5040	233	4.6
10 $Cd8^+Cd11c^+Klre1^+$	Parenchyma	18565	820	4.4
10 $Cd8^+Cd11c^+Klre1^+$	meninges	5040	154	3.1
11 $Cd8^+Ccr7^+Sell^+$	Parenchyma	18565	255	1.4
11 $Cd8^+Ccr7^+Sell^+$	meninges	5040	464	9.2
12 $Cd8^+Cx3cr1^+Gzma^+$	Parenchyma	18565	220	1.2
12 $Cd8^+Cx3cr1^+Gzma^+$	meninges	5040	353	7.0
13 $Cd4^+Foxp3^+$	Parenchyma	18565	286	1.5
13 $Cd4^+Foxp3^+$	meninges	5040	287	5.7
14 $Cd4^+Bcl3^+Relb^+$	Parenchyma	18565	317	1.7
14 $Cd4^+Bcl3^+Relb^+$	meninges	5040	50	1.0

$CD4^+$ T cell number per cluster in brain parenchyma (Fig. 3d)

Cluster	Replica	Total cell number	Cell number/Cluster
0 $Egr1^+$	Rep1	2319	319
0 $Egr1^+$	Rep1	2319	229
1 $Nkg7^+Ccl5^+$	Rep1	2319	171
1 $Nkg7^+Ccl5^+$	Rep2	2319	95
2 Rpl^+	Rep1	2319	409
2 Rpl^+	Rep2	2319	284

Author Manuscript Author Manuscript Author Manuscript Author Manuscript

Cluster	Replica	Total cell number	Cell number/Cluster
3 Slamf6$^+$Klf2$^+$	Rep1	2319	185
3 Slamf6$^+$Klf2$^+$	Rep2	2319	174
4 Cxcr6$^+$Ccr8$^+$	Rep1	2319	111
4 Cxcr6$^+$Ccr8$^+$	Rep2	2319	86
5 Foxp3$^+$	Rep1	2319	103
5 Foxp3$^+$	Rep2	2319	153

CD8$^+$ T cell number per cluster in brain parenchyma (Fig. 3g)

Cluster	Replica	Total cell number	Cell number/Cluster
0 Rpl$^+$	Rep1	9447	1526
0 Rpl$^+$	Rep2	9447	1444
1 Tox$^+$Pdcd1$^+$	Rep1	9447	932
1 Tox$^+$Pdcd1$^+$	Rep2	9447	829
2 Ly6c$^+$	Rep1	9447	510
2 Ly6c$^+$	Rep2	9447	457
3 Isg15$^+$	Rep1	9447	898
3 Isg15$^+$	Rep2	9447	750
4 Hobit$^+$Cd40lg$^+$	Rep1	9447	342
4 Hobit$^+$Cd40lg$^+$	Rep2	9447	167
5 Egr1$^+$	Rep1	9447	403
5 Egr1$^+$	Rep2	9447	304
6 Cd11c$^+$Klre1$^+$	Rep1	9447	221
6 Cd11c$^+$Klre1$^+$	Rep2	9447	100
7 Ccr7$^+$Sell$^+$	Rep1	9447	135
7 Ccr7$^+$Sell$^+$	Rep2	9447	77
8 Bcl3$^+$Relb$^+$	Rep1	9447	122
8 Bcl3$^+$Relb$^+$	Rep2	9447	114
9 Cx3cr1$^+$Gzma$^+$	Rep1	9447	88
9 Cx3cr1$^+$Gzma$^+$	Rep2	9447	28

Microglia number per cluster in brain parenchyma (Fig. 4a)

Cluster	Genotype	Replica	Total cell number	Cell number/Cluster	Percentage (%)
0 Homeostatic microglia	E4	Rep1	16951	16265	96.0
0 Homeostatic microglia	E4	Rep2	2901	2702	93.1
0 Homeostatic microglia	A/PE4	Rep1	7502	6072	80.9
0 Homeostatic microglia	TE4	Rep1	6210	4566	73.5
0 Homeostatic microglia	TE4	Rep2	3341	2061	61.7

Author Manuscript Author Manuscript Author Manuscript Author Manuscript

Cluster	Genotype	Replica	Total cell number	Cell number/Cluster	Percentage (%)
1 APOE$^+$ microglia	E4	Rep1	16951	455	2.7
1 APOE$^+$ microglia	E4	Rep2	2901	162	5.6
1 APOE$^+$ microglia	A/PE4	Rep1	7502	1206	16.1
1 APOE$^+$ microglia	TE4	Rep1	6210	1267	20.4
1 APOE$^+$ microglia	TE4	Rep2	3341	1137	34.0
2 IFN-activated microglia	E4	Rep1	16951	231	1.4
2 IFN-activated microglia	E4	Rep2	2901	37	1.3
2 IFN-activated microglia	A/PE4	Rep1	7502	224	3.0
2 IFN-activated microglia	TE4	Rep1	6210	377	6.1
2 IFN-activated microglia	TE4	Rep2	3341	143	4.3

Supplementary Material

Refer to Web version on PubMed Central for supplementary material.

Acknowledgement

We thank Justin Rustenhoven, Ben Korin and Asya Rolls for advice in single cell preparation; Xiaoqing Zhang and Shuhan Li for advice for scRNA-seq analysis; Diane Bender for assistance with multiplex immune monitoring; Maud Gratuze for PLX drug formulation. We thank Department of Pathology and Immunology Flow Cytometry and Fluorescence Activated Cell Sorting Core for help with cell sorting. This work was supported by a Carol and Gene Ludwig Award for Neurodegeneration Research (DMH), National Institute of Health grant NS090934 (DMH), the JPB Foundation (DMH), Cure Alzheimer's Fund (DMH) and Rainwater Charitable Foundation (DMH). MF was supported by the Ministry of Science and Higher Education of the Russian Federation (Agreement No. 075–15–2022–301). Single nuclei sequencing was performed at the McDonnell Genome Institute. Confocal microscopic analyses were performed at the Washington University Center for Cellular Imaging supported by Washington University School of Medicine, The Children's Discovery Institute of Washington University and St. Louis Children's Hospital (CDI–CORE–2015–505 and CDI–CORE–2019–813) and the Foundation for Barnes-Jewish Hospital (3770 and 4642). We thank Drs. Eric Reiman, Geidy Serrano, and Thomas Beach for human brain tissue. Schematic representation of fear conditioning behavioral paradigms (Fig.10i) were created by BioRender.

Reference

1. Duyckaerts C, Delatour B & Potier MC Classification and basic pathology of Alzheimer disease. Acta Neuropathol 118, 5–36, doi:10.1007/s00401-009-0532-1 (2009). [PubMed: 19381658]
2. Masters CL et al. Alzheimer's disease. Nat Rev Dis Primers 1, 15056, doi:10.1038/nrdp.2015.56 (2015). [PubMed: 27188934]
3. Jack CR Jr. & Holtzman DM Biomarker modeling of Alzheimer's disease. Neuron 80, 1347–1358, doi:10.1016/j.neuron.2013.12.003 (2013). [PubMed: 24360540]
4. Musiek ES & Holtzman DM Three dimensions of the amyloid hypothesis: time, space and 'wingmen'. Nat Neurosci 18, 800–806, doi:10.1038/nn.4018 (2015). [PubMed: 26007213]
5. Giannakopoulos P et al. Tangle and neuron numbers, but not amyloid load, predict cognitive status in Alzheimer's disease. Neurology 60, 1495–1500, doi:10.1212/01.wnl.0000063311.58879.01 (2003). [PubMed: 12743238]
6. Chen X & Holtzman DM Emerging roles of innate and adaptive immunity in Alzheimer's disease. Immunity 55, 2236–2254, doi:10.1016/j.immuni.2022.10.016 (2022). [PubMed: 36351425]
7. Ulrich JD et al. Altered microglial response to Abeta plaques in APPPS1–21 mice heterozygous for TREM2. Mol Neurodegener 9, 20, doi:10.1186/1750-1326-9-20 (2014). [PubMed: 24893973]

Author Manuscript Author Manuscript Author Manuscript Author Manuscript

8. Xiong M et al. APOE immunotherapy reduces cerebral amyloid angiopathy and amyloid plaques while improving cerebrovascular function. Sci Transl Med 13, doi:10.1126/scitranslmed.abd7522 (2021).
9. Rupp NJ, Wegenast-Braun BM, Radde R, Calhoun ME & Jucker M Early onset amyloid lesions lead to severe neuritic abnormalities and local, but not global neuron loss in APPPS1 transgenic mice. Neurobiol Aging 32, 2324 e2321–2326, doi:10.1016/j.neurobiolaging.2010.08.014 (2011).
10. Giannoni P et al. Cerebrovascular pathology during the progression of experimental Alzheimer's disease. Neurobiol Dis 88, 107–117, doi:10.1016/j.nbd.2016.01.001 (2016). [PubMed: 26774030]
11. Yoshiyama Y et al. Synapse loss and microglial activation precede tangles in a P301S tauopathy mouse model. Neuron 53, 337–351, doi:10.1016/j.neuron.2007.01.010 (2007). [PubMed: 17270732]
12. Long JM & Holtzman DM Alzheimer Disease: An Update on Pathobiology and Treatment Strategies. Cell 179, 312–339, doi:10.1016/j.cell.2019.09.001 (2019). [PubMed: 31564456]
13. Hammond TR, Marsh SE & Stevens B Immune Signaling in Neurodegeneration. Immunity 50, 955–974, doi:10.1016/j.immuni.2019.03.016 (2019). [PubMed: 30995509]
14. Heneka MT, Kummer MP & Latz E Innate immune activation in neurodegenerative disease. Nat Rev Immunol 14, 463–477, doi:10.1038/nri3705 (2014). [PubMed: 24962261]
15. Krasemann S et al. The TREM2-APOE Pathway Drives the Transcriptional Phenotype of Dysfunctional Microglia in Neurodegenerative Diseases. Immunity 47, 566–581 e569, doi:10.1016/j.immuni.2017.08.008 (2017). [PubMed: 28930663]
16. Mrdjen D et al. High-Dimensional Single-Cell Mapping of Central Nervous System Immune Cells Reveals Distinct Myeloid Subsets in Health, Aging, and Disease. Immunity 48, 380–395 e386, doi:10.1016/j.immuni.2018.01.011 (2018). [PubMed: 29426702]
17. Prinz M, Priller J, Sisodia SS & Ransohoff RM Heterogeneity of CNS myeloid cells and their roles in neurodegeneration. Nat Neurosci 14, 1227–1235, doi:10.1038/nn.2923 (2011). [PubMed: 21952260]
18. Fischer HG & Reichmann G Brain dendritic cells and macrophages/microglia in central nervous system inflammation. J Immunol 166, 2717–2726, doi:10.4049/jimmunol.166.4.2717 (2001). [PubMed: 11160337]
19. Gate D et al. CD4(+) T cells contribute to neurodegeneration in Lewy body dementia. Science 374, 868–874, doi:10.1126/science.abf7266 (2021). [PubMed: 34648304]
20. Zenaro E et al. Neutrophils promote Alzheimer's disease-like pathology and cognitive decline via LFA-1 integrin. Nat Med 21, 880–886, doi:10.1038/nm.3913 (2015). [PubMed: 26214837]
21. Subbarayan MS, Hudson C, Moss LD, Nash KR & Bickford PC T cell infiltration and upregulation of MHCII in microglia leads to accelerated neuronal loss in an alpha-synuclein rat model of Parkinson's disease. J Neuroinflammation 17, 242, doi:10.1186/s12974-020-01911-4 (2020). [PubMed: 32799878]
22. Garber C et al. T cells promote microglia-mediated synaptic elimination and cognitive dysfunction during recovery from neuropathogenic flaviviruses. Nat Neurosci 22, 1276–1288, doi:10.1038/s41593-019-0427-y (2019). [PubMed: 31235930]
23. Gate D et al. Clonally expanded CD8 T cells patrol the cerebrospinal fluid in Alzheimer's disease. Nature 577, 399–404, doi:10.1038/s41586-019-1895-7 (2020). [PubMed: 31915375]
24. Merlini M, Kirabali T, Kulic L, Nitsch RM & Ferretti MT Extravascular CD3+ T Cells in Brains of Alzheimer Disease Patients Correlate with Tau but Not with Amyloid Pathology: An Immunohistochemical Study. Neurodegener Dis 18, 49–56, doi:10.1159/000486200 (2018). [PubMed: 29402847]
25. Laurent C et al. Hippocampal T cell infiltration promotes neuroinflammation and cognitive decline in a mouse model of tauopathy. Brain 140, 184–200, doi:10.1093/brain/aww270 (2017). [PubMed: 27818384]
26. Lee SH et al. TREM2-independent oligodendrocyte, astrocyte, and T cell responses to tau and amyloid pathology in mouse models of Alzheimer disease. Cell Rep 37, 110158, doi:10.1016/j.celrep.2021.110158 (2021). [PubMed: 34965428]
27. Norris GT & Kipnis J Immune cells and CNS physiology: Microglia and beyond. J Exp Med 216, 60–70, doi:10.1084/jem.20180199 (2019). [PubMed: 30504438]

Author Manuscript Author Manuscript Author Manuscript Author Manuscript

28. Chen X et al. Transcriptomic mapping uncovers Purkinje neuron plasticity driving learning. Nature 605, 722–727, doi:10.1038/s41586-022-04711-3 (2022). [PubMed: 35545673]
29. Da Mesquita S, Fu Z & Kipnis J The Meningeal Lymphatic System: A New Player in Neurophysiology. Neuron 100, 375–388, doi:10.1016/j.neuron.2018.09.022 (2018). [PubMed: 30359603]
30. Da Mesquita S et al. Meningeal lymphatics affect microglia responses and anti-Abeta immunotherapy. Nature 593, 255–260, doi:10.1038/s41586-021-03489-0 (2021). [PubMed: 33911285]
31. Rustenhoven J & Kipnis J Bypassing the blood-brain barrier. Science 366, 1448–1449, doi:10.1126/science.aay0479 (2019). [PubMed: 31857468]
32. Rustenhoven J et al. Functional characterization of the dural sinuses as a neuroimmune interface. Cell 184, 1000–1016 e1027, doi:10.1016/j.cell.2020.12.040 (2021). [PubMed: 33508229]
33. Korn T & Kallies A T cell responses in the central nervous system. Nat Rev Immunol 17, 179–194, doi:10.1038/nri.2016.144 (2017). [PubMed: 28138136]
34. Siller-Farfan JA & Dushek O Molecular mechanisms of T cell sensitivity to antigen. Immunol Rev 285, 194–205, doi:10.1111/imr.12690 (2018). [PubMed: 30129204]
35. Loetscher M et al. Chemokine receptor specific for IP10 and mig: structure, function, and expression in activated T-lymphocytes. J Exp Med 184, 963–969, doi:10.1084/jem.184.3.963 (1996). [PubMed: 9064356]
36. Madore C, Yin Z, Leibowitz J & Butovsky O Microglia, Lifestyle Stress, and Neurodegeneration. Immunity 52, 222–240, doi:10.1016/j.immuni.2019.12.003 (2020). [PubMed: 31924476]
37. Gratuze M et al. Impact of TREM2R47H variant on tau pathology-induced gliosis and neurodegeneration. J Clin Invest 130, 4954–4968, doi:10.1172/JCI138179 (2020). [PubMed: 32544086]
38. Huang Y et al. Microglia use TAM receptors to detect and engulf amyloid beta plaques. Nat Immunol 22, 586–594, doi:10.1038/s41590-021-00913-5 (2021). [PubMed: 33859405]
39. Neefjes J, Jongsma ML, Paul P & Bakke O Towards a systems understanding of MHC class I and MHC class II antigen presentation. Nat Rev Immunol 11, 823–836, doi:10.1038/nri3084 (2011). [PubMed: 22076556]
40. Keren-Shaul H et al. A Unique Microglia Type Associated with Restricting Development of Alzheimer's Disease. Cell 169, 1276–1290 e1217, doi:10.1016/j.cell.2017.05.018 (2017). [PubMed: 28602351]
41. Mathys H et al. Temporal Tracking of Microglia Activation in Neurodegeneration at Single-Cell Resolution. Cell Rep 21, 366–380, doi:10.1016/j.celrep.2017.09.039 (2017). [PubMed: 29020624]
42. Filiano AJ et al. Unexpected role of interferon-gamma in regulating neuronal connectivity and social behaviour. Nature 535, 425–429, doi:10.1038/nature18626 (2016). [PubMed: 27409813]
43. Khalil M et al. Neurofilaments as biomarkers in neurological disorders. Nat Rev Neurol 14, 577–589, doi:10.1038/s41582-018-0058-z (2018). [PubMed: 30171200]
44. Pardoll DM The blockade of immune checkpoints in cancer immunotherapy. Nat Rev Cancer 12, 252–264, doi:10.1038/nrc3239 (2012). [PubMed: 22437870]
45. Sharpe AH & Pauken KE The diverse functions of the PD1 inhibitory pathway. Nat Rev Immunol 18, 153–167, doi:10.1038/nri.2017.108 (2018). [PubMed: 28990585]
46. Rosenzweig N et al. PD-1/PD-L1 checkpoint blockade harnesses monocyte-derived macrophages to combat cognitive impairment in a tauopathy mouse model. Nat Commun 10, 465, doi:10.1038/s41467-019-08352-5 (2019). [PubMed: 30692527]
47. Baruch K et al. PD-1 immune checkpoint blockade reduces pathology and improves memory in mouse models of Alzheimer's disease. Nat Med 22, 135–137, doi:10.1038/nm.4022 (2016). [PubMed: 26779813]
48. Kumagai S et al. The PD-1 expression balance between effector and regulatory T cells predicts the clinical efficacy of PD-1 blockade therapies. Nat Immunol 21, 1346–1358, doi:10.1038/s41590-020-0769-3 (2020). [PubMed: 32868929]
49. Turley SJ, Fletcher AL & Elpek KG The stromal and haematopoietic antigen-presenting cells that reside in secondary lymphoid organs. Nat Rev Immunol 10, 813–825, doi:10.1038/nri2886 (2010). [PubMed: 21088682]

Author Manuscript Author Manuscript Author Manuscript Author Manuscript

50. Kigerl KA, de Rivero Vaccari JP, Dietrich WD, Popovich PG & Keane RW Pattern recognition receptors and central nervous system repair. Exp Neurol 258, 5–16, doi:10.1016/j.expneurol.2014.01.001 (2014). [PubMed: 25017883]

51. Huynh TV et al. Lack of hepatic apoE does not influence early Abeta deposition: observations from a new APOE knock-in model. Mol Neurodegener 14, 37, doi:10.1186/s13024-019-0337-1 (2019). [PubMed: 31623648]

52. Noguchi T et al. Temporally Distinct PD-L1 Expression by Tumor and Host Cells Contributes to Immune Escape. Cancer Immunol Res 5, 106–117, doi:10.1158/2326-6066.CIR-16-0391 (2017). [PubMed: 28073774]

53. Wozniak DF et al. Motivational disturbances and effects of L-dopa administration in neurofibromatosis-1 model mice. PLoS One 8, e66024, doi:10.1371/journal.pone.0066024 (2013). [PubMed: 23762458]

54. Yuede CM et al. Behavioral consequences of NMDA antagonist-induced neuroapoptosis in the infant mouse brain. PLoS One 5, e11374, doi:10.1371/journal.pone.0011374 (2010). [PubMed: 20613880]

55. Khuchua Z et al. Deletion of the N-terminus of murine map2 by gene targeting disrupts hippocampal ca1 neuron architecture and alters contextual memory. Neuroscience 119, 101–111, doi:10.1016/s0306-4522(03)00094-0 (2003). [PubMed: 12763072]

56. Hammond TR et al. Single-Cell RNA Sequencing of Microglia throughout the Mouse Lifespan and in the Injured Brain Reveals Complex Cell-State Changes. Immunity 50, 253–271 e256, doi:10.1016/j.immuni.2018.11.004 (2019). [PubMed: 30471926]

Author Manuscript Author Manuscript Author Manuscript Author Manuscript

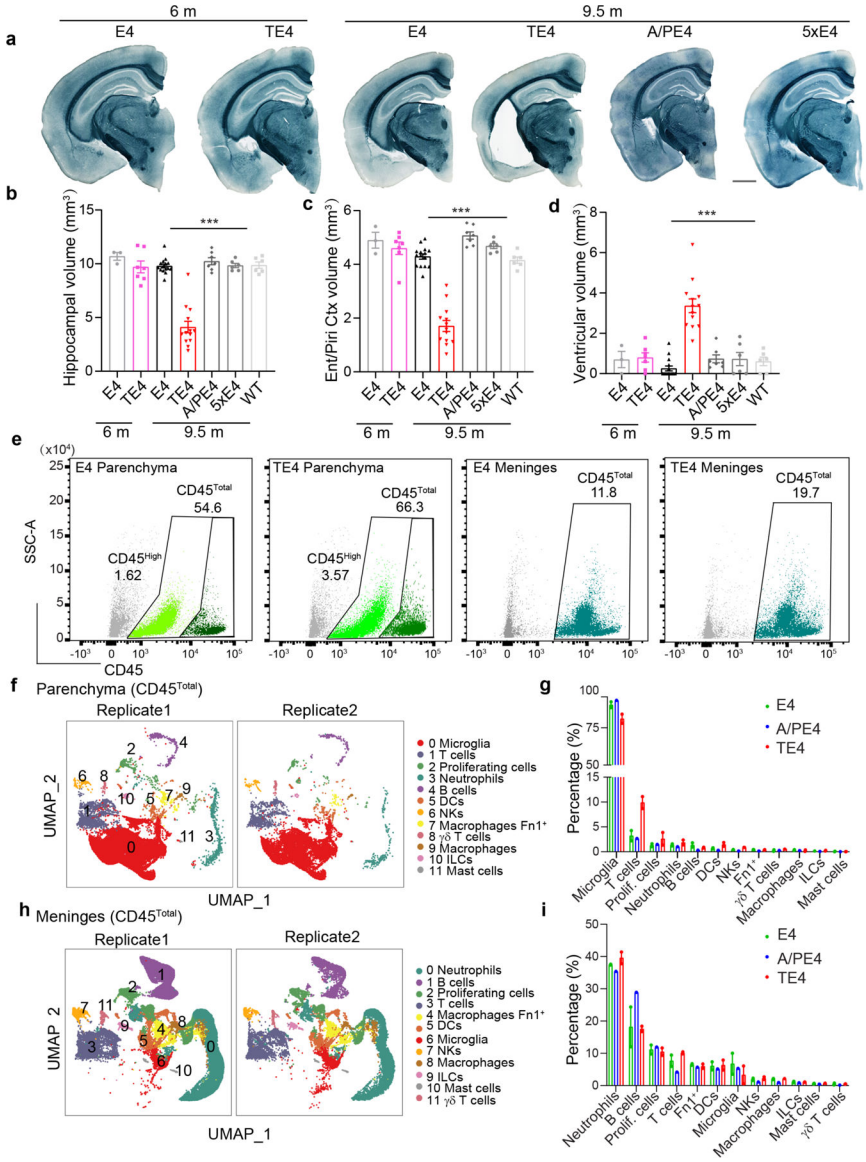

Figure 1. Single cell immune RNA sequencing reveals increased proportion of T cells in the context of tau-mediated neurodegeneration

(**a**) Representative images of 6-month E4 and TE4; 9.5-month E4, TE4, A/PE4 and 5xE4 mouse brain sections stained with Sudan black. Scale bar=1mm. (**b-d**) Volumes of hippocampus, entorhinal/piriform cortex and posterior lateral ventricle in 6-month E4 and TE4; 9.5-month E4, TE4, A/PE4, 5xE4 and WT mice. (E4–6m: n=3, TE4–6m: n=7, E4–9.5m: n=15, TE4–9.5m n=13, A/PE4–9.5m: n=7, 5xE4–9.5m: n=6 and WT-9.5m: n=6). Data are mean ± s.e.m.; ***p<0.0001 for 9.5m, TE4 *vs.* A/PE4; TE4 *vs.* 5xE4; TE4 *vs.* E4 and TE4 *vs.* WT. Ent: Entorhinal. Piri: Piriform. One-way ANOVA with Tukey's post hoc test. (**e**) FACS sorting of $CD45^{Total}$ and/or $CD45^{high}$ cells from brain parenchyma and meninges from E4, A/PE4 and TE4 mice for single cell immune RNA-seq. (**f**) $CD45^{Total}$ immune cells from brain parenchyma assigned into 12 cell types as visualized by UMAP plot. (**g**) Bar plot showing the proportions of the 12 cell types of immune cells in the brain parenchyma. Data are mean ± s.e.m.; 2 biologically independent samples were utilized and

Author Manuscript Author Manuscript Author Manuscript Author Manuscript

samples were sequenced in n=2 batches from the E4 and TE4 groups. (**h**) $CD45^{Total}$ immune cells from meninges assigned into 12 cell types as visualized by UMAP plot. (**i**) Bar plot showing the proportions of the 12 cell types of immune cells in the meninges. Data are mean ± s.e.m.; 2 biologically independent samples were utilized and samples were sequenced in n=2 batches from the E4 and TE4 groups.

Author Manuscript Author Manuscript Author Manuscript Author Manuscript

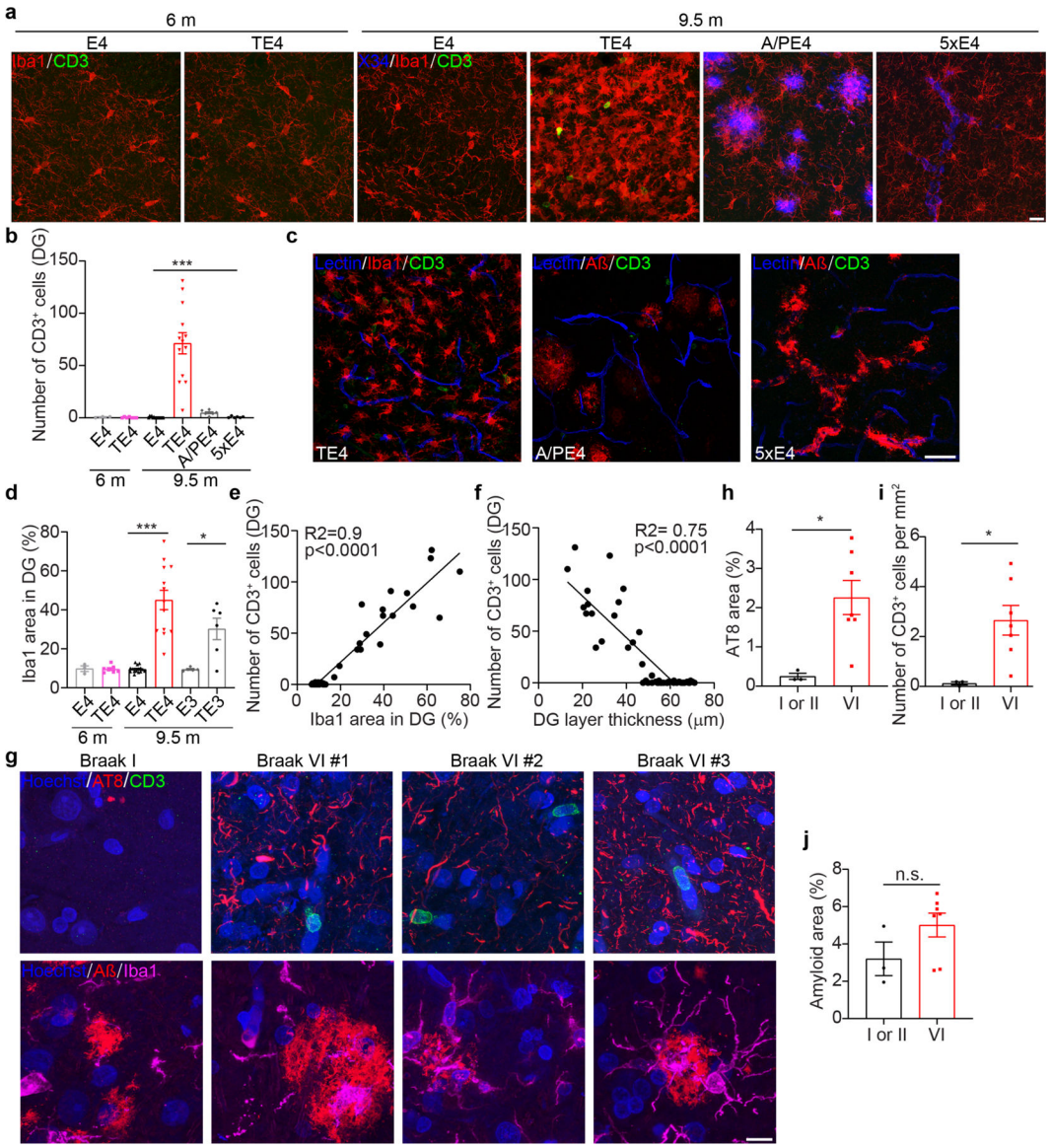

Figure 2. T cells are strongly elevated in the brain parenchyma of humans and mice with tauopathy and neuronal loss

(**a**) Iba1 and CD3 staining in 6-month E4 and TE4, 9.5-month E4, TE4, A/PE4 and 5xE4 mice in dentate gyrus (DG). Scale bar=20µm. (**b**) Quantification of numbers of $CD3^+$ T cells in DG per $0.3mm^2$. (E4–6m: n=3, TE4–6m: n=7, E4–9.5m: n=15, TE4–9.5m: n=13, A/PE4–9.5m: n=7 and 5xE4–9.5m: n=6). ***p<0.0001 for 9.5m, TE4 *vs.* A/PE4; TE4 *vs.* 5xE4 and TE4 *vs.* E4. One-way ANOVA with Tukey's post hoc test. (**c**) Vessel and CD3 staining in 9.5-month TE4, 19-month A/PE4 and 5xE4 mice, Scale bar=20µm. (**d**) Quantification of the % area covered by Iba1 in DG. (E4–6m: n=3, TE4–6m: n=7, E4–9.5m: n=15, TE4–9.5m n=13, E3–9.5m: n=5 and TE3–9.5m: n=6). ***p<0.0001 for TE4–9.5m *vs.* E4–9.5m; and *p=0.0276 for TE3–9.5m *vs.* E3–9.5m. One-way ANOVA with Tukey's post hoc test. (**e**) Correlation between the area covered by Iba1 and number of $CD3^+$ T cells. n=49 biologically independent animals from d. Pearson correlation analysis (two-sided). R^2=0.902, p<0.0001. (**f**) Correlation between the number of $CD3^+$ T cells

Author Manuscript Author Manuscript Author Manuscript Author Manuscript

with the granule cell layer thickness in DG. n=49 biologically independent animals from d. Pearson correlation analysis (two-sided). R^2=0.7454. p<0.0001. (**g**) CD3, Aβ and AT8 staining in brain sections from AD patients (superior frontal gyrus) of low Braak stage I or II and high Braak stage VI. Scale bar=10μm. (**h**) Quantification of the area covered by AT8 in g. (Braak I or II: n=3; Braak VI: n=7). n refers to staining quantification from brain of individual humans. *p=0.0195. Unpaired two-tailed Student's *t* test. (**i**) Quantification of numbers of $CD3^+$ T cells per mm^2 in h. *p=0.0277. Unpaired two-tailed Student's *t* test. (**j**). Quantification of the area covered by Aβ in h. (Braak I or II: n=3; Braak VI: n=7). n refers to staining quantification from brain of individual humans. p=0.1522. Data are mean ± s.e.m.; Unpaired two-tailed Student's *t* test.

Author Manuscript Author Manuscript Author Manuscript Author Manuscript

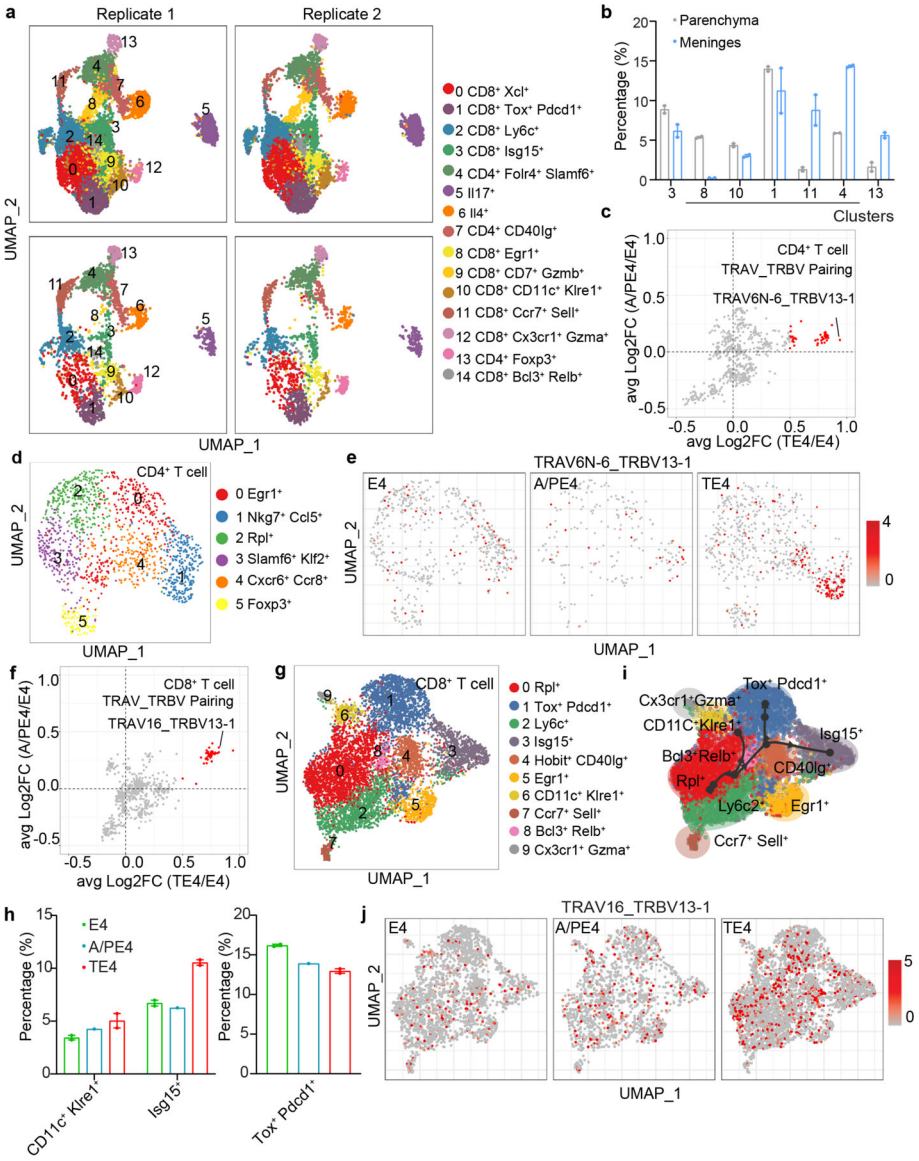

Figure 3. T cells dynamically shift from activated to exhausted states with unique TCR clonal expansion in tauopathy

(**a**) Total T cells from brain parenchyma and meninges assigned into 15 categories as visualized by UMAP plot. (**b**) Bar plot showing the percentages of T cells subgroups in E4, A/PE4 and TE4 mice. Data are mean ± s.e.m.; 2 biologically independent samples were utilized and samples were sequenced in n=2 batches from the E4 and TE4 groups. (**c**) Scatter plot illustrating differential TRAV and TRBV pairing expression in $CD4^+$ T cells in TE4 *vs.* E4 (x axis) and A/PE4 *vs.* E4 (y axis) mice. (**d**) $CD4^+$ T cells from brain parenchyma assigned into 6 cell types as visualized by UMAP plot. (**e**) Representative TRAV-TRBV paring projection in $CD4^+$ T cells in E4, A/PE4 and TE4 mice. (**f**) Scatter plot illustrating differential TRAV and TRBV pairing expression in $CD8^+$ T cells in TE4 *vs.* E4 (x axis) and A/PE4 *vs.* E4 (y axis) mice. (**g**) $CD8^+$ T cells from brain parenchyma assigned into 10 cell types as visualized by UMAP plot. (**h**) Percentages of activated (cell types 3 and 6) and exhausted (cell type 1) $CD8^+$ T cells in E4, A/PE4 and TE4 mice. Data are mean ± s.e.m.; 2

Author Manuscript Author Manuscript Author Manuscript Author Manuscript

biologically independent samples were utilized and samples were sequenced in n=2 batches from the E4 and TE4 groups. (**i**) Trajectory analysis showing naive $CD8^+$ T cells demarcated into three paths, cell type 6, $Itgax^+$ $Klre1^+$; cell type 3, $ISg15^+$ and cell type 1, Tox^+ $Pdcd1^+$. (**j**) Representative TRAV-TRBV pairing projection in $CD8^+$ T cells in E4, A/PE4 and TE4 mice.

Author Manuscript Author Manuscript Author Manuscript Author Manuscript

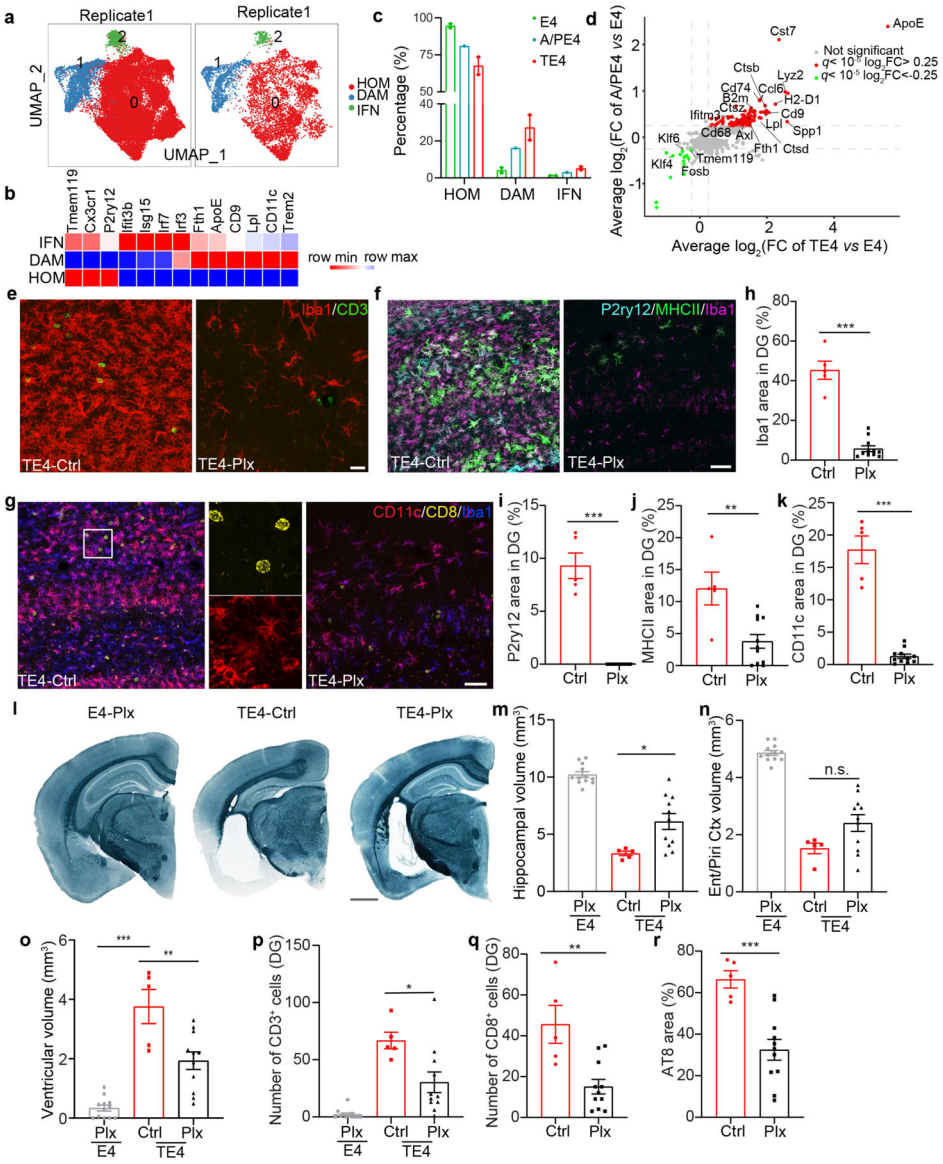

Figure 4. Microglia depletion prevents T cell infiltration in tauopathy

(**a**) Total microglia assigned into 3 subgroups, HOM, DAM and IFN activated microglia, as visualized by UMAP plot. (**b**) Heat map showing representative markers specifically expressed in 3 subgroups. (**c**) Bar plot showing the percentages of the 3 subgroups of microglia in E4, A/PE4 and TE4 mice. Data are mean ± s.e.m.; 2 biologically independent samples were utilized and samples were sequenced in n=2 batches from the E4 and TE4 groups. (**d**) DEGs in microglia subgroups. FC, fold change. (**e**) Iba1 and CD3 staining in 9.5-month TE4 mice. Scale bar=20μm. (**f**) P2ry12, MHCII and Iba1 staining in 9.5-month TE4 mice. Scale bar=50μm. (**g**) CD11c, CD8 and Iba1 staining in 9.5-month TE4 mice. Scale bar=50μm. (**h-k**) Quantification of the covered areas of Iba1, P2ry12, MHCII and CD11c in 9.5-month mice. (TE4-Ctrl: n=5 and TE4-Plx: n=11). ***p<0.0001, ***p<0.0001, **p=0.0031, ***p<0.0001 for TE4-Plx *vs.* TE4-Ctrl for Iba1, P2ry12, MHCII and CD11c, respectively. Unpaired two-tailed Student's *t* test. (**l**) Representative images of

Author Manuscript Author Manuscript Author Manuscript Author Manuscript

9.5-month mouse brain sections stained with Sudan black. Scale bar=1mm. (**m-o**) Volumes of hippocampus, entorhinal/piriform cortex and posterior lateral ventricle in 9.5-month mice. (E4-Plx: n=12; TE4-Ctl: n=5 and TE4-Plx: n=11). **p=0.0078 **p=0.0012, for TE4-Ctrl *vs.* TE4-Plx for volumes of hippocampus and posterior lateral ventricle, respectively. One-way ANOVA with Tukey's post hoc test. (**p**) Quantification of the number of $CD3^+$ T cells in DG per $0.3mm^2$ in 9.5-month mice. (E4-Plx: n=12; TE4-Ctl: n=5 and TE4-Plx: n=11). *p=0.0236 for TE4-Ctrl *vs.* TE4-Plx. Unpaired two-tailed Student's *t* test. (**q**) Quantification of the number of $CD8^+$ T cells in DG per $0.3mm^2$ in 9.5-month mice. (TE4-Ctrl: n=5 and TE4-Plx: n=11). **p=0.002 for TE4-Ctrl *vs.* TE4-Plx. (**r**) Quantification of the area covered by AT8 in DG per slice in 9.5-month mice. (TE4-Ctrl: n=5 and TE4-Plx: n=11). ***p=0.0008 for TE4-Ctrl *vs.* TE4-Plx. Unpaired two-tailed Student's *t* test. Data in h-k, m-r are mean ± s.e.m.

Author Manuscript Author Manuscript Author Manuscript Author Manuscript

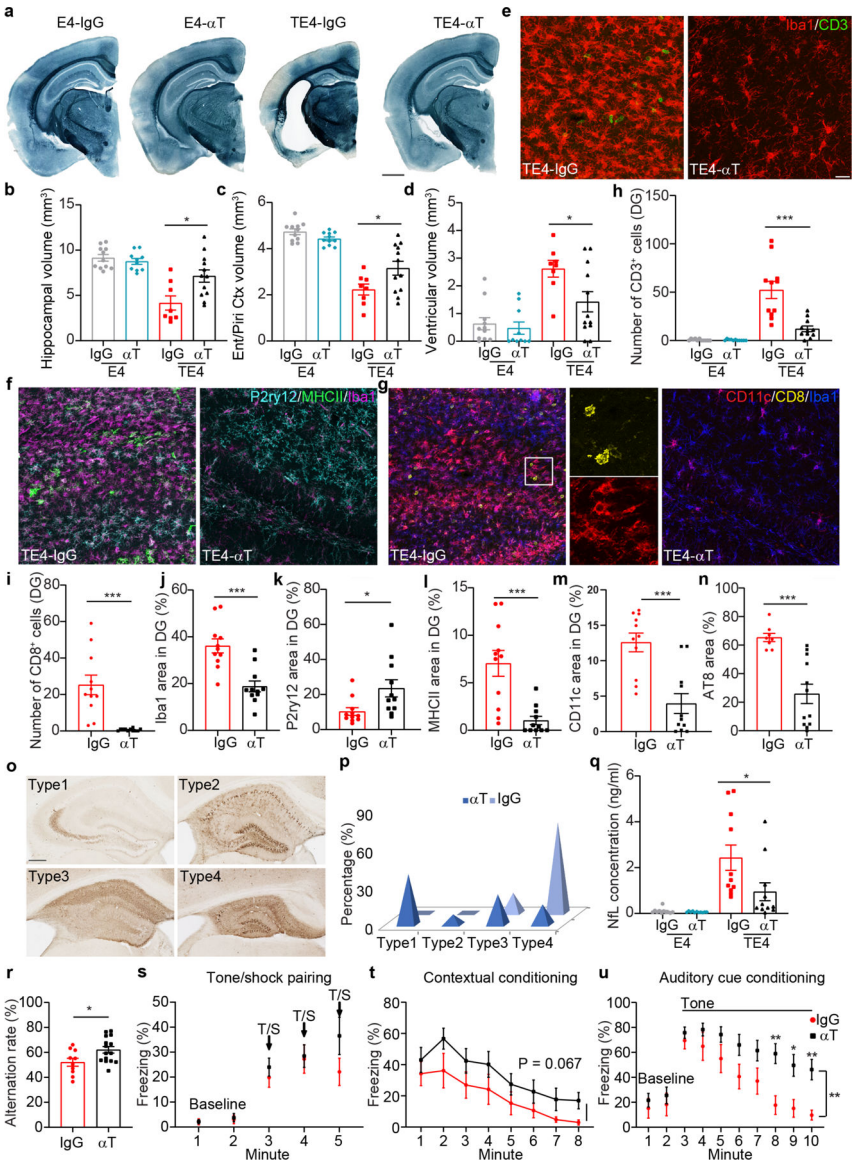

Figure 5. Depletion of T cells ameliorates inflammation, tauopathy, brain atrophy, and improves behavior

(**a**) Representative images of 9.5-month brain sections. Scale bar=1mm. (**b-d**) Volumes of brain regions in 9.5-month mice. (E4-IgG: n=11; E4-αT: n=10; TE4-IgG: n=8 and TE4-αT: n=12). *p=0.0112, *p=0.0397, *p=0.0313 for TE4-IgG *vs.* TE4-αT for hippocampus, entorhinal/piriform cortex and posterior lateral ventricle, respectively. Unpaired two-tailed Student's *t* test. (**e**) Iba1 and CD3 staining in 9.5-month mice. Scale bar=20μm. (**f**) P2ry12, MHCII and Iba1 staining in 9.5-month mice. Scale bar=50μm. (**g**) CD11c, CD8, Iba1 staining in 9.5-month mice. Scale bar=50μm. (**h**) Quantification of $CD3^+$ T cells in DG per $0.3mm^2$ in 9.5-month mice. (E4-IgG: n=11; E4-αT: n=11; TE4-IgG: n=11 and TE4-αT: n=11). ***p=0.0004. Unpaired two-tailed Student's *t* test. (**i**) $CD8^+$ T cells per $0.3mm^2$ of DG in 9.5-month mice. (TE4-IgG: n=11 and TE4-αT: n=11). ***p=0.0002. Unpaired two-tailed Student's *t* test. (**j-n**) Quantification of the immunostained areas in 9.5-month mice. (TE4-IgG: n=11 and TE4-αT: n=11, for j-m and TE4-IgG: n=8, TE4-αT: n=12 for

Author Manuscript Author Manuscript Author Manuscript Author Manuscript

n). ***p=0.0002, *p=0.0229, ***p=0.0004, ***p=0.0002, ***p=0.0002 for area of Iba1, P2ry12, MHCII, CD11c and AT8, respectively. Unpaired two-tailed Student's *t* test. (**o**) Distinct p-Tau staining patterns. **p=0.007 for distribution between TE4-IgG and TE4-αT. Fisher's exact test. (**p**) Percentage of p-Tau staining patterns in 9.5-months mice. (**q**) Plasma NfL concentration in 9.5-month mice. (E4-IgG: n=11; E4-αT: n=11; TE4-IgG: n=11 and TE4-αT: n=11). *p=0.0398. Unpaired two-tailed Student's *t* test. (**r**) Y maze behavior in 8.5-month mice. (TE4-IgG: n=10 and TE4-αT: n=15). *p=0.0239. Unpaired two-tailed Student's *t* test. (**s**) Tone/shock pairing, day 1. (TE4-IgG: n=10 and TE4-αT: n=15). p=0.2152. Two-way ANOVA, with Bonferroni post hoc comparisons test. (**t**) Freezing in response to contextual cue, day 2. (TE4-IgG: n=10 and TE4-αT: n=15). p=0.067. Two-way ANOVA, with Bonferroni post hoc comparisons test. (**u**) Freezing in response to auditory cue, day 3. (TE4-IgG: n=10 and TE4-αT: n=15). **p=0.0118. Two-way ANOVA, with Bonferroni post hoc comparisons test. Data in b-h, i-n, q-u are mean ± s.e.m.